View Article Online / Journal Homepage / Table of Contents for this issue
Dynamic Article Links

Soft Matter

Cite this: *Soft Matter*, 2012, **8**, 1275

www.rsc.org/softmatter

REVIEW

Structure and functionality of edible fats

Alejandro G. Marangoni,*[a] Nuria Acevedo,[a] Fatemeh Maleky,[a] Edmund Co,[a] Fernanda Peyronel,[a] Gianfranco Mazzanti,[b] Bonnie Quinn[c] and David Pink[c]

Received 30th June 2011, Accepted 11th October 2011
DOI: 10.1039/c1sm06234d

Fat-structured food materials are an important component of our diet. The role that fat plays in material functionality, flavor perception, texture and health characteristics is due in large part to its physical properties. An understanding of these physical properties is relevant from scientific, technological and medical perspectives. The physical properties of fat materials, are, in turn, governed by a complex confluence of the various structural levels in a fat material beginning with triglyceride molecules. The formation of nanoscale structural elements by these molecules is the first step in the formation of a fat material as we know it. This review shows how these microstructural elements can be imaged and characterized. It is also shown that the formation of these nanocrystals is affected by the attendant crystallization parameters. Through simulation and a discussion of van der Waals forces, it is shown that these nanoscale elements assemble into colloidal aggregates with fractal character. The influence of microstructure on the mechanical properties of a fat material is explained using a variety of mechanical models. Lastly, this review examines methods by which the properties and characteristics of the various structural levels can be engineered. Shear has been shown to affect the polymorphism and phase transition kinetics of triglyceride crystals. As well, shear has been shown to modify the aggregation of nanocrystals, with consequences for the porosity and diffusivity of oil through the fat crystal network.

[a]*Dept. of Food Science, University of Guelph, Guelph, ON, Canada. E-mail: amarango@uoguelph.ca*
[b]*Dept. of Process Engineering & Applied Science, Dalhousie University, Halifax, NS, Canada*
[c]*Dept. of Physics and Astronomy, St Francis Xavier University, Antigonish, NS, Canada*

1. Introduction

The texture, mouthfeel, flavor and other sensory characteristics of foods are a strong function of the nano- and meso-scale structure, structural failure and flow characteristics, as well as the

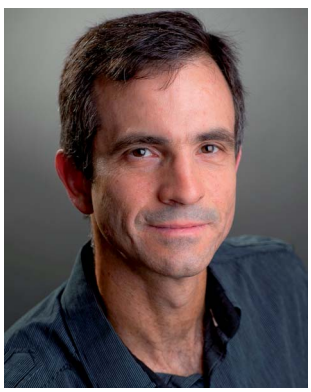

Alejandro G. Marangoni

Dr Alejandro Marangoni is a professor and Canada Research Chair in Food and Soft Materials Science in the Department of Food Science at the University of Guelph. His work concentrates on the materials science of foods, particularly fat crystallization and structure, as well as the relationship between food structure and physiological response in humans. His work continues to focus on establishing quantitative relationships between macroscopic functionality and the appropriate length scale within a material. Current research focuses on food nanostructure, better understanding the nature of van der Waals forces at the nanoscale, as well as polymer gelation of anhydrous aliphatic oils.

Nuria Acevedo

Dr Nuria Acevedo is a post-doctoral research associate at the University of Guelph, Canada. She received her PhD in Food Science from the University of Buenos Aires, Argentina. Her current research focuses on the nanotechnology of fat food products for the enhancement of human health; in particular the effects of external fields on fat crystallization and structure at the nanoscale and their relationship to specific macroscopic properties. The aim of this work is to open up the possibility of engineering the nanostructure of fats to target specific functionalities such as mechanical strength, spreadability and oil binding capacity.

Published on 11 November 2011. Downloaded by Michigan State University on 19/01/2016 06:25:56.

View Article Online

Published on 11 November 2011. Downloaded by Michigan State University on 19/01/2016 06:25:56.

melting behavior of an underlying elastoplastic fat crystal network within foods.[1–4] This is particularly the case for "fatty" foods such as chocolate, butter, ice-cream, whipped cream, croissants (and most laminated bakery products), to name a few. The reason for our great delight in consuming fat has been linked to the primordial survival of our species, and most other mammals for that matter—fat is the most energy dense macronutrient, providing 9 kcal g^{-1} of energy, as opposed to a "meager" 4 kcal g^{-1} for carbohydrates and protein. No other macronutrient packs more energy per gram than fats. In addition, fat is hydrophobic, that is, it does not bind water as proteins and polysaccharides do. Thus, the storage of fat in tissues does not upset the osmotic balance of cells, allowing substantial quantities of fat to be stored within specialized tissues.

From an applied perspective, the motivation for studying fat structure and function is two-fold. From an industrial viewpoint, an in-depth knowledge of the molecular structure, crystallization behavior, rheological properties, nano- and meso-scale structure of fats is necessary for the rational design and engineering of food materials. As is the case for numerous industrial soft materials (such as plastics and rubber), structure–function relationships need to be developed in order to optimize and improve manufacturing processes as well as to develop new applications for these materials. The second motivation for studying fats is

Fatemeh Maleky

Dr Fatemeh (Farnaz) Maleky received her Bachelor's degree in Chemical Engineering in 1994 from Isfahan University of Technology, Iran and her Master's and PhD degrees in Food Science in 2007 and 2011, respectively, from University of Guelph, Canada. She is currently a postdoctoral researcher in the Department of Food Science, University of Guelph, Canada. Her research focuses on the area of lipid crystallization, particularly fat nanotechnology for improved health and sensory attributes of food materials. Dr Maleky has several patents and publications and is the recipient of numerous awards and honors including an NSERC CGS award from the Government of Canada.

Fernanda Peyronel

Ms Fernanda Peyronel has an MSc degree in Atomic and Molecular Physics from the University of Guelph and a Licenciatura en Fisica from the University of Rosario, Argentina. She is currently a Research Associate in the Food and Soft Materials Science at the University of Guelph, as well as working on her PhD. Her current interests include the quantification of London–van der Waals interactions between fat crystals at both nano-scale and micro-scale using Lifshitz theory. Her experimental focus is on building devices for the accurate determination of the static dielectric constant of materials.

Mr Edmund Co graduated in Food Science from the University of Guelph in 2008. He obtained his MSc in Food Chemistry from the University of Guelph in 2011. He currently works as a Research Associate/Lecturer at the University of Guelph. His scientific interests focus primarily on the study of food structure in relation to food functionality as well as alternative lipid structurants.

Gianfranco Mazzanti

Dr Gianfranco Mazzanti is an Associate Professor at Dalhousie University. He is a chemical engineer with an MSc in food processing engineering, PhD in Food Science and postdoctoral experience in Physics. Dr Mazzanti has pioneered the understanding of crystallization of triglycerides under shear, introducing detailed analysis of synchrotron X-ray diffraction data obtained under shear flow. He has developed a physical understanding, along with its corresponding mathematical models, that have brought on a new way of looking at the nanostructure and microstructure of crystalline fats. He has built novel Rheo-NMR instrumentation allowing the unprecedented quantification of crystallization under shear flow.

 This journal is © The Royal Society of Chemistry 2012

View Article Online

Published on 11 November 2011. Downloaded by Michigan State University on 19/01/2016 06:25:56.

related to the health consequences of our excessive love for consuming fat-rich foods. We are currently experiencing an explosion in the incidence of obesity in societies both rich and poor. This is due to the ready availability of highly refined, energy-dense foods. For example, with close to 35% of the U.S. adult population and 20% of U.S. children being clinically obese,[5] we are witnessing an unprecedented increase in the incidence of type-II diabetes and cardiovascular disease. This increase in morbidity will have tremendous implications for the future of countries with universal medical care policies. An overburdened medical care system will draw funds away from initiatives in education, the environment, science and technology and the arts. The heavy costs associated with "diseases of affluence" could seriously jeopardize many future-building endeavors. Arguably, on a societal scale, much more could be achieved by improving the health characteristics of the foods we consume than by pharmaceutical intervention—it is easier and much less expensive to eat less sugary drinks, less fatty foods and more fiber than to inject insulin into our bloodstream or take atorvastatin (Lipitor™) to decrease serum cholesterol levels. The challenge thus is to produce low-calorie foods containing less "bad fats" while retaining many of the quality characteristics historically associated with a particular food. It is a proven fact that people will not consume a particular food if it does not meet certain sensory expectations, regardless of health benefits. Having set the stage, the purpose of this short review is to appraise the reader of the current state of knowledge in the materials science of edible fats. Some recent advances in attempts at improving the health characteristics of fats in foods will also be highlighted.

What is fat?

Fats and oils are complex multi-component mixtures of triacylglycerols. Triacylglycerols (TAGs) are tri-esters of glycerol and fatty acids. Fatty acids can have chain lengths ranging from 4 carbons, such as butyric acid, to 22 carbons with six double bonds, such as docosahexaenoic acid (DHA). The unsaturation of the fatty acids plays a key role in the physical and nutritional functionality of TAGs. Triglycerides with saturated and/or longer chain fatty acids will have higher melting points than triglycerides composed predominantly of shorter chain and/or unsaturated fatty acids. This brings us to the subtle difference between a fat and an oil. The only difference between the two is that fat is solid at ambient/room temperatures (25 °C) while oil is liquid. It would thus be reasonable to predict that oils such as olive, sunflower, canola and soybean will contain a greater proportion of mono and polyunsaturated fatty acids, while fats such as milk fat, cocoa butter and palm fat will contain a greater proportion of saturated fatty acids. A point to remember is that homogeneous TAGs (such as tristearin and tripalmitin) are uncommon in nature and that most TAG molecules are heterogeneous and will contain fatty acids of differing unsaturation and chain length within the same molecule. Should this not be complicated enough, the positional distribution of fatty acids within the TAG molecule is regiospecific; that is, the esterified fatty acids tend to occupy primarily one of the three sites on the glycerol backbone, *i.e.*, *sn*-1, *sn*-2 or *sn*-3. For example, the short-chained butyric acid (butanoic acid in IUPAC nomenclature) occupies the *sn*-3 position in milk fat preferentially, while the *sn*-2 position in cocoa butter is populated almost exclusively by oleic acid (*cis*-9-18:1, octadecenoic acid). From a nutritional perspective, consumption of poly-unsaturated fatty acids, instead of carbohydrate, is associated with improved cardiovascular health while consumption of *trans*-fatty acids is associated with an increased risk of developing cardiovascular diseases.[6–11]

Crystallization behavior, solid state structure and structural hierarchy

Fats are polycrystalline materials: TAG crystals scatter X-rays and have defined melting points. Upon cooling a TAG melt below the crystallization temperature of the highest melting TAG or TAG compound (TAGs display a rich phase behavior in the solid state), the melt becomes undercooled with the result that the

Ms Bonnie Quinn has a BSc in Mathematics and a BEd. She has been in David Pink's research group at St Francis Xavier University for over 25 years as a principal software designer, and is now the Senior Research Associate. She plays a major role in teaching undergraduates how to write code in order to simulate coarse-grained models of biological systems. She also helps direct them in their research work. As an integral member of the research group she has co-authored about 30 papers with other group members. She has been a member of the Advanced Food Materials Network (AFMNet) since its inception.

David Pink

Dr David Pink is Physics Senior Research Professor at St Francis Xavier University and is in the third era of his research career. His early research was in magnetically ordered systems and cooperative phenomena using analytical methods. He moved into the field of biological membranes and lipid bilayers with occasional excursions into other directions, most recently into bacterial outer membranes and biofilms. At that time he introduced computer simulation into his work. His association with AFMNet led to his third-era interest in fats and oils and aggregation for which he extended his techniques to atomic scale MD. He uses dissipative particle dynamics to model fluid flow.

View Article Online

Published on 11 November 2011. Downloaded by Michigan State University on 19/01/2016 06:25:56.

highest-melting TAG becomes supersaturated within a metastable region with respect to the liquid phase in which it is now dissolved. As is the case for melts, the driving force for this particular liquid–solid phase transitions is the chemical potential difference ($\Delta\mu$) between a TAG molecule in the liquid state (melt or solution) and in the solid state, $\Delta\mu = RT\ln\beta$, where the supersaturation ratio $\beta = [c]/[c^*]$, contrasts the solubility of a molecule in the melt $[c]$ relative to its solubility limit $[c^*]$ at a particular temperature and pressure. For melts of pure substances, $\Delta\mu$ can be conveniently described in terms of the undercooling as $\Delta\mu = \Delta H_m(T_m - T)/T$, where ΔH_m (J mol^{-1}) and T_m (K) represent, respectively, the melting enthalpy and melting point of the TAG species crystallizing at a particular temperature, T. The supersaturation of the melt is a very important parameter which will greatly affect both nucleation and crystal growth processes. Of great consequence to the crystallization of TAGs is the fact that TAGs undergo metastable nucleation. Depending on the supersaturation of the melt, TAGs can crystallize into one of three predominant forms, α, β′ and β, in ascending order of melting point, density and stability. Each one of these forms is accessible directly from the melt. However, homotropic polymorphic phase transformations from a less stable (β′) solid phase to a more stable solid phase (β) will take place in time. TAG nucleation into a particular polymorphic form is easily understood using activation energy arguments. The energy of activation to form the α form is much lower than the activation energy to form the β′ or β forms. Its formation will be kinetically favored even though the complete opposite is the case in terms of thermodynamic stability.[12] This metastable nucleation behavior arises due to the relatively large characteristic time required for proper molecular alignment and packing upon nucleation since the long hydrocarbon fatty acid chains in the TAG can adopt a large number of conformations, *i.e.*, are very flexible, with no global free energy minimum for a particular conformation in the molten state. This fact can be easily demonstrated by carrying out a simple molecular mechanics (MM2 or similar routines) simulation on any TAG molecule.

TAG nucleation has been found to obey the Gibbs–Thompson model, which predicts the Gibbs free energy change associated with the formation of a crystal embryo (ΔG_n). The model includes free energy contributions from both surface (positive) and volume changes (negative) and is defined by $\Delta G_n = A_n\gamma - V_n(\Delta\mu/V_m^s)$, where A_n is the surface area of a nucleus, γ is the surface free energy per unit area, V_n is the volume of a nucleus, $\Delta\mu$ is the chemical potential difference between the solid and liquid phases (related to the degree of supersaturation) and $V_m{}^s$ is the molar volume of the solid.[13] The formation of a fat crystal leads to the creation of a solid–liquid interface, resulting in an unfavorable positive contribution to the free energy of nucleation (proportional to A_n). On the other hand, the formation of a crystal simultaneously leads to a decrease in the chemical potential difference between the solid and liquid phases (proportional to V_n). The stability of a nucleus is thus governed by a characteristic dimension, to which both the interfacial area and nucleus volumes scales accordingly. Thus, at a critical nucleus size (r_c), a maximum in the free energy-nucleus size profile will be observed, where an increase proportional to A_n is exactly balanced by a decrease proportional to V_n. Beyond r_c, the free energy of nucleation will continuously decrease. In order to minimize their free energy, clusters smaller than r_c will breakdown, and those larger than r_c will continue to grow. The quantification of the free energy of activation for nucleation in TAGs can thus be readily determined using the Fisher–Turnbull[14] approach from knowledge of the nucleation rate (approximated as the inverse of the induction time for nucleation, τ, at different temperatures):

$$\ln\ (\tau T) = -\ln\ \frac{\alpha N k_B}{h} + \frac{16\pi\gamma^3\left(V_m^s\right)^2 T_m^2}{3k_B\Delta H_m^2}\left(\frac{1}{T(\Delta T)^2}\right) \quad (1)$$

Thus, a plot of $\ln\ (\tau T)$ *versus* $1/[T(\Delta T)^2]$ should yield a straight line with a slope, m (K^3), which equals:

$$m = \frac{16\pi\delta^3\left(V_m^s\right)^2 T_m^2}{3k_B\Delta H_m^2} \quad (2)$$

where k_B corresponds to Boltzmann's constant and γ is the crystal-melt surface energy (or interfacial tension), N is Avogadro's number, h is Planck's constant (J s), T_m is the melting point of the solid (K), ΔH_m is the enthalpy of melting of the solid (J mol^{-1}), while ΔT is the temperature difference between the melting point of the solid T_m and the temperature at which isothermal crystallization is taking place—this is the degree of undercooling (K).

The free energy of nucleation (J per nucleus) can then be determined from:

$$\Delta G_n^{r_c} = \frac{mk_B}{(\Delta T)^2} \quad (3)$$

This approach is also used for the determination of the crystal-melt interfacial tension, γ, of fats using a rearranged version of eqn (2).[15,16]

Fat crystallization is dominated by nucleation processes. Knowledge of this initial step in the formation of a fat crystal network is critical—crystal size (and by extension, the number of crystals), spatial distribution of mass and crystal surface characteristics are highly dependent on the nucleation rate. For example, Marangoni and McGauley[17] reported that the degree of space-filling of crystalline mass in a cocoa butter crystal network was a function of the nucleation rate. This degree of fill strongly influences the mechanical properties of a fat material.[18–21]

When TAG crystals nucleate, molecules adopt "tuning fork" (*sn*-1 and *sn*-3 fatty acids in the *Z*-conformation, in the same orientation relative to the glycerol plane), or "chair" (*sn*-1 and *sn*-2 fatty acids in the *Z*-conformation, in the same orientation relative to the glycerol plane) conformations upon packing into a crystalline lattice (Fig. 1). Since in the solid state, the fatty acid hydrocarbon chains are generally in an extended, all-*trans* conformation, this results in a very long *c*-axis of the unit cell relative to the small *a* and *b* short axes. This molecular asymmetry results in the formation of distinct TAG crystalline lamellae upon crystallization. Depending on the type of TAG stacking in the lamellae, which can be described as "back-to-back" or "seat-to-seat", different long axis dimensions as a multiple of the chain lengths are possible: two[22–24] ($2L$), three[25,26] ($3L$) and even four[27,28] ($2L \times 2$) fatty acid chain lengths long. As stated before, the high molecular flexibility of the hydrocarbon chains opens up the possibility for different packing modes which can be characterized using wide angle

 This journal is © The Royal Society of Chemistry 2012

View Article Online

Published on 11 November 2011. Downloaded by Michigan State University on 19/01/2016 06:25:56.

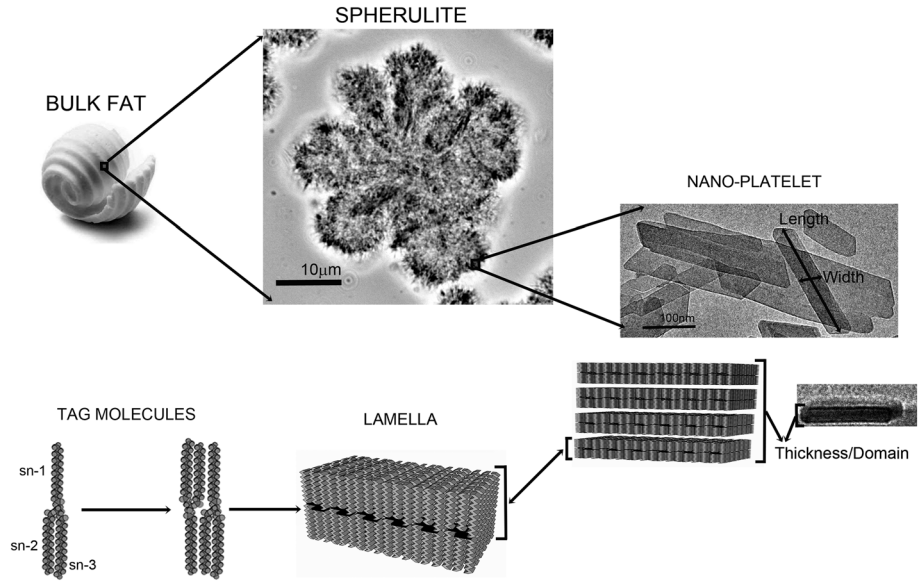

Fig. 1 An updated structural hierarchy of a triacylglycerol crystal network. A bulk fat consists microstructurally of spherulites, which are in turn, composed of crystalline nanoplatelets assembled from crystalline lamellae of triglycerides.

powder X-ray diffraction. The packing arrangement of ethylene groups within the long fatty acid chains can be described using a "subcell" concept, in contrast to the unit cell of the entire crystal. The subcell structures of the α, β′ and β polymorphic forms have been associated with hexagonal, orthorhombic and triclinic packing arrangements of ethylene asymmetric units, each with its own characteristic powder XRD patterns. Even though it is very convenient to consider a TAG crystal as a collection of hydrocarbon chains, this predicted subcell structure is different from the unit cell structure. For example, single crystal studies on the β′ and β forms of many TAGs show a monoclinic unit cell structure. No indexing studies exist mainly due to the very low number of peaks obtained from spectra. Much more fundamental research is required in this area.

The study of TAG polymorphism is the most active area of research in this field due to its implications for nucleation behavior and crystal growth, which, in turn, will affect the final crystallite size and network structure, both of which will, in their turn, affect the mechanical properties and melting behavior of a fat. TAG polymorphism is particularly critical in chocolate manufacture. Six different polymorphs have been identified for cocoa butter. However, only one of these polymorphs will result in chocolate with desirable sensory qualities. The so-called Form V can be identified by its characteristic small-angle spacing (a $3L$ lamellar tuning fork structure with $d_{001} \cong 64$ Å), its wide angle X-ray scattering patterns (triclinic polyethylene packing) and narrow melting range (32–34 °C), close to the temperature of the mouth. Much effort is devoted to attaining this particular polymorphic crystal form during chocolate manufacture. Chocolate tempering techniques are designed to promote the formation of Form V seed crystals. Transformation from Form V to Form VI will result in an unacceptable chocolate with a high melting point. When consumed, Form VI cocoa butter will coat the inside of the mouth and will not melt. This results in a waxy sensation. Moreover, transformation of Form V cocoa butter to Form VI due to poor storage conditions will result in the appearance of large crystals on the surface of the chocolate. This will result in surface roughening.[29] These crystals will scatter light diffusely, leading to the formation of white "bloom" on the surface of the chocolate, with obvious quality and economic losses. Excessive temperature cycling and the presence of liquid oil in the form of a confectionery filling (as in the case of truffles), alcohol, or any fat solvent will exacerbate this process. The topic of triglyceride polymorphism is and has been a very active area of research in this field. Many excellent reviews have been written on the topic. Due to space limitations, we will not cover triglyceride solid state structure and polymorphism in this review. Much early work is summarized in the book by Donald Small.[30] An excellent review of the area is given by Kiyotaka Sato.[31]

The nucleation of TAGs is quickly followed by crystalline growth. At the mesoscale level (length scales within the micrometre range), we can witness a very diverse assortment of crystal habits—spherulites, needle-like crystals, microplatelets, disordered crystal aggregates, spherical crystal aggregates, fractal-like aggregates, and even some morphologies that defy proper description. Despite the wide variety of crystal morphologies, they all share some common attributes: (1) the structures are awe-inspiringly beautiful when viewed under a polarized light microscope and (2) the crystalline mass in a network of these crystals is distributed in a fractal fashion. Crystalline growth of TAG molecules can be considered to follow the Avrami model as adapted to the study of the kinetics of fat crystallization,[12] $(\mathrm{SFC}/\mathrm{SFC}_{\max}) = 1 - \mathrm{e}^{-k_{\mathrm{A}}t^{n}}$, where SFC is the solid fat content (the mass fraction of crystalline material determined by pulsed NMR) while the Avrami constant, k_{A} is a kinetic rate constant for growth. The Avrami exponent, n, describes the dimensionality of growth and the type of nucleation, as per the original theory.

The polycrystals or crystal aggregates observed under the polarized light microscope do not constitute the primary crystals

View Article Online

Published on 11 November 2011. Downloaded by Michigan State University on 19/01/2016 06:25:56.

formed upon nucleation. The formation of these polycrystals is strongly influenced by external fields (such as temperature gradients and shear fields) experienced during nucleation and the early stage of growth. Just recently, our group managed to isolate and identify the primary crystals that make up these larger polycrystals and crystal aggregates.[5,6] The discovery and characterization of these asymmetric nanoplatelets will be described fully in Section 2. Armed with this new knowledge of an underlying structure of nanoplatelets at the foundation of our material microstructure, we are currently actively engaged in trying to understand the aggregation mechanisms responsible for the formation of mesoscale structures. Our most current attempts are highlighted in Section 3 of this review. Molecular van der Waals (vdW) forces play a key role in the aggregation of these nanoplatelets into larger clusters. Colloidal vdW forces govern the interactions between nanoplatelet clusters, which eventually lead to the formation of a fat crystal network. Section 4 of the review will summarize our efforts of the past three years in the quantification of van der Waals forces using Lifshitz theory. In Section 5, we will describe a structural-mechanical model which relates the primary crystal size, strength of van der Waals interactions, solid fat content and the spatial distribution of network mass to the mechanical properties of fats. Section 6 will describe the use of fields, particularly shear flow fields to engineer the crystal properties (*i.e.* crystal habit and polymorph) of fat crystal networks. Section 7 will discuss recent advances of how fat crystal network structure affects the migration of oil through the network, which will lead to material softening and re-crystallization, *e.g.*, bloom formation.

In order to properly set the stage for the sections to follow, we will leave you with Fig. 1, which summarizes the structure of fats at different length scales, from TAG molecules, primary nanoplatelets, and mesocrystals, to a colloidal network of polycrystals. The macroscopic properties of a fat, including mechanical strength, oil binding capacity, and sensory properties are a function of a complex combination of the material structural properties at different length scales. However, the level of structure that directly affects the macroscopic properties is the meso-scale structure. We will thus start with a view of the microstructure and the recently discovered nanoplatelets that make up this microstructure.

2. Mesoscale and nanoscale structure

The microstructural level, *i.e.*, the mesoscale, of the fat crystal network may be defined as those structures in the length range between 1 μm and 200 μm and the interactions between these structures. At the lower range of the microstructural level, one encounters individual crystallites, whilst at the upper ranges, one decidedly is observing aggregates of microstructural elements (clusters of crystallites). Work from our laboratories has shown that the polycrystals observed under a polarized light microscope are actually fractal crystal aggregates and that fat mechanical properties can be modelled by considering fat to be a close-packed system of near-spherical polycrystalline clusters (or spherulites).[18,19] Mechanical yielding in such a system comes from the stretching of links between relatively "hard" flocs. This regime is thus called the "weak-link" regime. Thus, fat can be considered to be a colloidal gel of small primary particles aggregating into clusters, or flocs. What was not proven until last year was what constituted a primary particle. As a matter of fact, in this area of research, crystal clusters in the 5–20 μm range were usually considered as the primary crystals of the polycrystalline network. These crystals were generally accepted to be the smallest particles observed under the ubiquitous polarized light microscope. Fat crystals are birefringent and thus appear bright under polarized light against a backdrop of non-birefringent and dark oil. Yet, our work regarding the effects of shear on fat crystal networks hinted that the crystals observed under a polarized light microscope were not the smallest microstructural element in a fat crystal network. Our data strongly suggested the existence of a platelet with dimensions in the hundred-nanometre range.[32,33] This idea was bolstered last year upon publication of the first characterization of the sub-micron, or for lack of a better word, the nanoscale, of fat crystal networks.[34,35] The challenge of this work was to directly observe and quantify the primary crystal size in the presence of liquid oil. Since cryogenic electron microscopy had to be used for this purpose to avoid melting, direct observation of the material was not possible. Liquid oil crystallizes at cryogenic temperatures and thus the contrast between the oil and the fat is very poor. Single nanocrystals had therefore to be extracted from the crystal clusters and liquid oil had to be removed, preferably with minimal damage to the primary crystal structure.

Early attempts to remove oil included the use of aqueous detergent solutions such as Teepol[36] and Aerosol OT,[37] or solvents which did allow unique observations of near-single crystals platelets to be made.[38] Furthermore, Chawla and deMan described a method focused on the use of isobutanol as a solvent to dissolve and hence remove the liquid phase without dissolving the solid fat.[39]

Even though TAG nano-crystals formed in colloidal suspensions of organic solvents have been observed by TEM,[40,41] the work reported by Heertje and Leunis[42] was the first to visualize and quantify native platelet-like fat crystals using Transmission Electron Microscopy (TEM). However, the origin of the observed platelet structure and its place within the structural hierarchy of a native fat crystal network was not clear until our characterization was published. We had to develop a sample treatment for disrupting the fat crystal network and removing entrapped liquid oil with cold isobutanol (10 °C) in order to visualize single nanocrystal units *via* cryogenic-TEM. Armed with this extraction technique, we proceeded to systematically characterize this level of structure in TAG crystal networks. Moreover, the possibility of engineering the nanostructure of such materials and therefore its functionality at the macroscopic level was considered for the first time.

As mentioned earlier, upon crystallization, TAG molecules stack in lamellae (Fig. 1). The height of an individual lamella corresponds to the long axis (*c*-axis) of the unit cell of a TAG crystal as determined from small angle powder XRD. Fig. 2 shows a cryo-TEM image of the crosssection of a primary nanocrystal. It can be clearly seen from the image that each single nanoplatelet is composed of stacked TAG lamellae. In this image it was possible to visualize the internal structure of the nanoplatelets. Furthermore, the reported data of lamellar dimensions and the value of the crystallographic angle in the *ab* plane (~60°) are in close agreement with powder XRD data.

 This journal is © The Royal Society of Chemistry 2012

View Article Online

Published on 11 November 2011. Downloaded by Michigan State University on 19/01/2016 06:25:56.

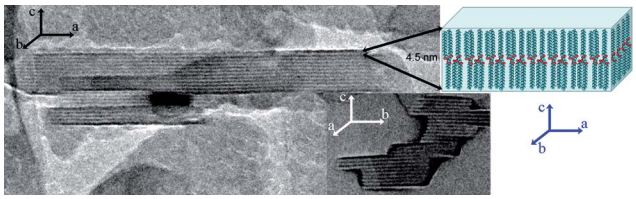

Fig. 2 A cryo-TEM micrograph showing "side views" of 2 nanoplatelets formed by tristearin obtained from fully hydrogenated canola oil (FHCO). The striations within the nanoplatelet suggest the formation of lamellae by the TAG molecules. The distance between each line corresponds to an individual TAG lamella, in this case approximately 4.5 nm. The epitaxial growth of these TAG lamellae (approximately 7 to 10 layers thick) results in the formation of a nanoplatelet.

The epitaxial stacking of several lamellae leads to the creation of crystalline domains. The thickness of the domains corresponds to the thickness of the nanoplatelets. This thickness can be determined *via* Scherrer analysis of the small-angle X-ray diffraction data.[43] A comprehensive and updated representation of the different structural levels present in a fat crystal network has been recently published.[44] The following work incorporates the recent electron microscopic work conducted in our lab.

It has been extensively shown that the structure of most processed food depends not only on the chemical composition, but also on the processing history of the material.[45] Several investigations have demonstrated that processing conditions including cooling and shear rates during crystallization, storage time and temperature, among numerous others, affect the crystalline structure and therefore the functional properties of fats and fat-structured food materials. In addition, changes in the matrix supersaturation induce variations in the microstructure of TAG networks; *i.e.* a decrease in supersaturation is manifested as a reduction in the crystal cluster size and network density.[16,46,47]

Using the extraction method described above, we succeeded in demonstrating that external fields can affect the nanoscale of triacylglycerol crystal networks.[35,48,49] Fig. 3 is a collection of cryo-TEM micrographs obtained for fully hydrogenated canola oil (FHCO) crystallized under static conditions and with a slow cooling rate of 1 °C min^{-1} (Fig. 3A). In addition, images of the same sample were taken after dilution with high oleic sunflower oil (HOSO) in a 1 : 1 ratio (Fig. 3B), and after changes in the crystallization conditions: a fast cooling rate of 10° min^{-1} (Fig. 3C) and a laminar shear rate of 300 s^{-1} (Fig. 3D). Corresponding frequency distributions of the mean values of the nanocrystal dimensions are also displayed in Fig. 3. It is evident that the length and width of the nanoplatelets increased when the matrix supersaturation was halved (Fig. 3A and B). In addition, the crystalline domain size, determined by small-angle X-ray diffraction, also increased with a decrease in supersaturation. The results demonstrate that in a more dilute sample, nanoplatelet sizes are more than twice than those observed in the undiluted FHSO sample. On the other hand, both high cooling and shear rates induced the formation of smaller nanoplatelets ($p < 0.001$). A fast cooling rate during crystallization induced a platelet size decrease in FHSO of ~13% for length, ~5% for width and ~12% for thickness (data not shown) relative to the dimensions of nanoplatelets crystallized at a slow cooling rate. As well, nano-scale characterization of the sheared FHCO samples revealed that the application of laminar shear during crystallization led to a 7% decrease in platelet lengths and a 5% decrease in the platelet widths. The effect of shear was particularly pronounced when the supersaturation of the system was reduced *via* dilution with oil.

3. Assembly of fat nanoparticles—the formation of polycrystalline crystal clusters

It is highly likely that the recently discovered fat nanostructure described above, with a characteristic length scale of ~100 nm, represents the fundamental structural unit in crystalline fats. With this in mind, we now turn our attention to how the steady state structure of a nanoplatelet aggregate arises. This will allow us to better appreciate the roles of the crystal nanoplatelet as a structural building block of fat systems. There are two approaches to tackling the problem of how nanoplatelets assemble in polycrystalline aggregates: (i) experimental data gathering in which a mathematical model is used to organize and understand the experimental data and (ii) predictions of mathematical models in cases for which little data is available. Since we are at the very early stages of our understanding of how nanoplatelet aggregation leads to the creation of the mesoscale structure, we will describe the equilibrium and/or steady state structural properties of these fat crystalline nanoplatelets (CNP)[35] embedded in oil using mathematical models. The term *platelet aggregation* is more widely used to describe the aggregation of blood platelets *via* chemical interactions in a flowing fluid.[50,51] In that case, it is essential that the models include the walls of the blood vessels. Here, the oil is not necessarily flowing and there are no necessary constraining walls. It is these two points which differentiate nanoplatelet aggregation in oils from blood platelet aggregation inside blood vessels.

The molecular constituents of the CNPs and the oils considered here are triacylglycerols (TAGs). They undergo an order–disorder phase transition at a temperature, T_m, between a solid crystalline phase and a fluid phase together with restructuring transitions involving the symmetry of the crystal lattice at temperatures less than T_m. In the absence of boundaries, the fluid appears to be isotropic. We shall identify aspects of these systems which are likely to, at least partly, determine their larger-scale characteristics, followed by a description of the mathematical models of CNPs, and predictions over a range of spatial scales.

Structural model of a fat nanocrystal and its interactions

A TAG crystalline nanoplatelet (CNP) is highly anisotropic with two of its spatial dimensions being ~10 times larger than the third.[35] If we identify the "unit" structures with which to build up the CNPs, we then need only to establish the interaction between a pair of unit structures belonging to different CNPs in order to deduce the interaction between a pair of CNPs. Because of the spatial scale, it is unrealistic to use TAG molecules as the unit structures and, instead, we use a continuum solid shape to represent a collection of TAG molecules. Bearing in mind TAG polymorphism, the unit structures could be rhombohedral or orthorhombic in shape, each representing a volume of TAG molecules in their extended chain states with a packing density characteristic of a particular crystalline phase. Each CNP would

View Article Online

Published on 11 November 2011. Downloaded by Michigan State University on 19/01/2016 06:25:56.

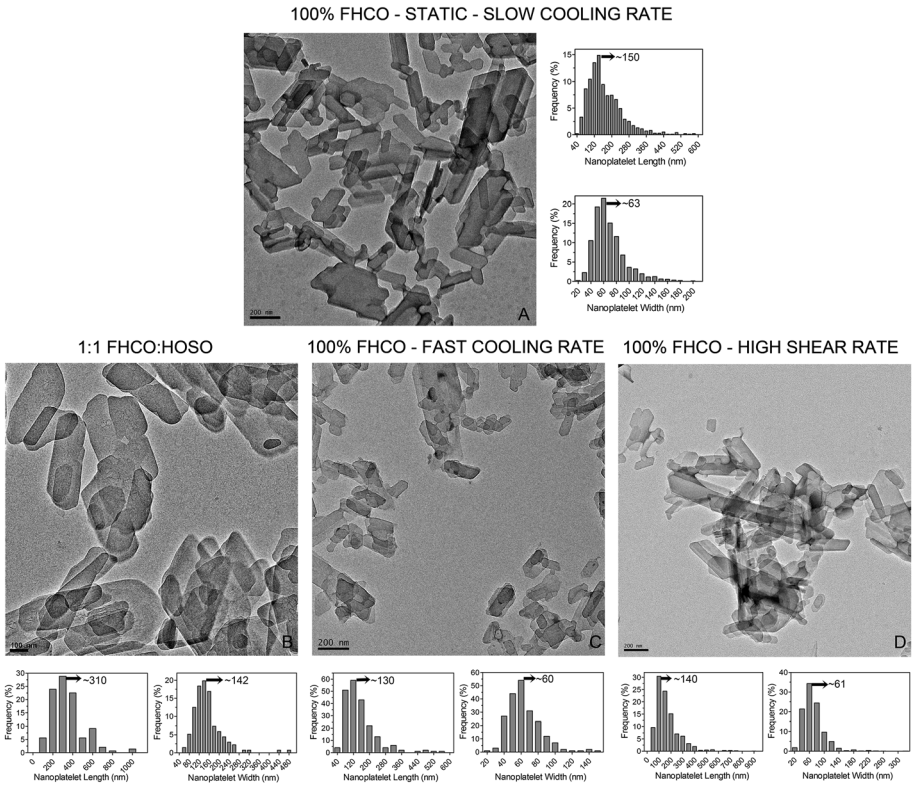

Fig. 3 Cryo-TEM micrographs and nanoplatelet size distributions of tristearin (FHCO) crystallized under various conditions. (A) Static crystallization of tristearin from the melt at a low cooling rate (1 °C min^{-1}). (B) Static crystallization of tristearin from a triolein solution (tristearin : triolein 1 : 1) at a low cooling rate (1 °C min^{-1}). (C) Static crystallization of tristearin from the melt at a high cooling rate (10 °C min^{-1}). (D) Crystallization of tristearin from the melt at a low cooling rate (1 °C min^{-1}) under a laminar shear rate of 300 s^{-1}.

then be composed of a close-packed array of such structures. However, it is not simple to calculate an analytical form of the attractive dispersion interaction between rhombohedral and orthorhombic structures for arbitrary relative orientations and a given centre-of-mass (COM) separation. It is more convenient to represent each CNP as a close-packed structure of spheres, since the attractive part of the dispersion interactions between spheres has been established.[52,53] Each sphere, representing a continuum of TAG molecules with a density characteristic of the crystalline phase of interest, possesses radius R, and the collection of spheres forms the CNP. Fig. 4 shows a CNP described as a collection of spheres.

We assume that each sphere in a CNP interacts attractively with another sphere from a different CNP *via* a dispersion interaction potential:[52]

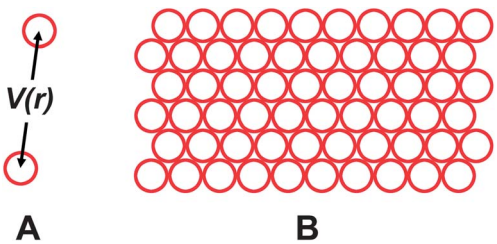

Fig. 4 (A) Two spheres, belonging to different CNPs, interact *via* $V(r)$. (B) A CNP for which $m = 10$ and $n = 6$.

$$V(r) = V_A(r),\ r > 2R + \delta \tag{4}$$

$$V(r) = -V_0,\ r \le 2R + \delta \tag{5}$$

$$V_A(r) = -\frac{A}{6}\left[\frac{2R^2}{f_1} + \frac{2R^2}{f_2} + \ln\left(\frac{f_1}{f_2}\right)\right] = -\frac{A}{6}\left[2R^2\left(\frac{1}{f_1} + \frac{1}{f_2}\right) + \ln\left(\frac{f_1}{f_2}\right)\right] \tag{6}$$

$$f_1 = s^2 + 4Rs \tag{7}$$

$$f_2 = s^2 + 4Rs + 4R^2 = (s + 2R)^2 \tag{8}$$

$$s = r - 2R \tag{9}$$

where R is the radius of the spheres, r is the center-to-center distance between the two spheres, A is the Hamaker coefficient (see "Dispersion forces in fats and oils" section), δ is a small distance, s is the shortest distance between the surfaces of two spheres for a given r, and V_0 is the binding energy per pair of spheres belonging to different nanocrystals. In order to create a nanocrystal for computer simulation, spheres are packed on a rigid $m \times n$ 2-dimensional hexagonal lattice to create an object, of dimension $m \times n \times 1$ shown in Fig. 4. When two spheres belonging to different CNPs are sufficiently close to each other, defined by a characteristic distance, δ, they become "bound" with a binding energy, $-V_0$.

 This journal is © The Royal Society of Chemistry 2012

View Article Online

Published on 11 November 2011. Downloaded by Michigan State University on 19/01/2016 06:25:56.

The value of the Hamaker coefficient, common to all cases, was estimated from (a) the length scale of the system, *viz.*, the size of a sphere and (b) the composition of the nanocrystals and the medium. To do so, we made use of GROMACS parameters.[54] GROMACS is an atomic scale molecular dynamics package described in the next section (Dispersion forces in fats and oils).

Two limiting CNP interaction regimes were considered. In a weak interaction regime, the binding energy V_0 possesses a value $\sim k_B T$ so that thermal fluctuations can bring about aggregate structural relaxation. In a strong interaction regime, $V_0 \gg k_B T$. In this regime, no rearrangement or reorientation is possible after two CNPs have become bound.

A Monte Carlo technique utilizing the Metropolis algorithm[55] was employed to model the aggregation of N CNPs, each of size $m \times m \times 1$, in an $L \times L \times L$ simulation box with periodic boundary conditions. The Metropolis algorithm defines a sequence of states of a system such that probability distributions can be calculated from it. The algorithm comprises the following steps. Consider a system in an initial state possessing energy E_i. Let us attempt to change the state randomly, and let the new (final) state possess energy E_f. Define $\Delta E = E_f - E$. (i) If $\Delta E \leq 0$ then the change is accepted and the system is in the new state with energy E_f. (ii) If $\Delta E > 0$, then we choose a random number, y, with $0 \leq y < 1$. (iii) If $y \leq e^{-\beta \Delta E}$, $\beta^{-1} = k_B T$ where k_B is Boltzmann's constant and T is the absolute temperature, then the system is in the new state. (iv) Otherwise the system remains in the initial state. It can be proven that for the systems described here, the final distribution will be characteristic of a system in thermodynamic equilibrium. The simulated CNPs were allowed to change their state as required by the Metropolis algorithm, by translating and rotating with respect to their centres of mass, with the attractive part of the interaction (eqn (4)) turned off. After the simulated CNPs had relaxed, the interaction (eqn (4)) was turned on and the Metropolis algorithm used so that the collection of CNPs was allowed to come to thermal equilibrium or to a steady state. In this procedure, the movement of clusters of CNPs was included. Movement of clusters was permitted with a translational step size as well as an angle of rotation around a randomly chosen axis through the centre of mass, by an amount proportional to $M^{-1/2}$, where M is the mass of the cluster. The population of CNPs was also simulated as a Gaussian distribution with mean size $= m \times m \times 1$.

The structure function $S_f(\vec{q})$ is a quantity that has been widely used to characterize the average structures of aggregates.[56,57] The (static) structure function $S_f(\vec{q})$ is defined as:

$$S_f(\vec{q}) = \frac{1}{N}\left|\sum_j f(\vec{r}_j)\exp\ i(\vec{q}\ \vec{r}_j)\right|^2 = \frac{1}{N}\sum_j \sum_k f(\vec{r}_j) f(\vec{r}_k)^* \exp i\left(\vec{q}\ (\vec{r}_j - \vec{r}_k)\right) \quad (10)$$

where the sums over j and k range over all objects, $f(\vec{r}_j)$ is associated with the sphere located at position $\vec{r}_j$ and * indicates a complex conjugate. The vector $\vec{q}$ (magnitude q) is a wavevector. If we are simulating X-ray (neutron) diffraction, then $S_f(\vec{q}) = I(\vec{q})$, the scattering intensity, $f(\vec{r}_j)$ is the electron density (neutron scattering length) of the atom (nucleus) at $\vec{r}_j$, and q is related to the X-ray wavelength, λ, and the scattering angle of the X-rays, 2θ, by $q = (4\pi/\lambda)\sin\theta$. The structure can be studied simply by putting all $f(\vec{r}_j) = 1$. If we average $S_f(\vec{q})$ over all vectors $\vec{q}$ possessing a fixed magnitude, $|\vec{q}| = q$,

$$S_f(q) = \langle S_f(\vec{q})\rangle_{|\vec{q}|=q} \quad (11)$$

then we obtain a "powder pattern". The structure function will exhibit peaks at lengths, l, characteristic of the system with $l = 2\pi/q$. Furthermore, if the system exhibits fractal characteristics with dimension D, then one will find a region of q-space for which $S_f(q) \approx q^{-D}$ for a sufficiently large range of q.

The results of the CNP aggregation simulation are shown in Fig. 5. In this example, the simulation box size was $L = 50$ units, the diameter of each sphere was 1 unit with all CNPs equal in size and shape and with $m = n = 10$. There were three CNP mass concentrations, 6%, 11% and 20%. We also simulated a Gaussian distribution of CNPs possessing mean values of $m = n = 10$, variance, $\sigma^2 = 5$, and a mass concentration of 11%. We initialized the system with the attractive interactions switched off, then switched on the interactions (eqn (4)–(9)) and allowed the system to aggregate.

Fig. 5 yields four messages: (i) instantaneous snapshots of the results show that, while the weak interaction regime gives rise to "multilayer sandwiches", which eventually form a single sandwich, the strong interaction regime quickly results in a single extended cluster with no apparent preferred orientation of the CNPs. (ii) the "Bragg peaks" (log $[q] \approx 1$) identifying characteristic lengths are identical for both interactions. (iii) Whether all CNPs are of equal size or whether there is a Gaussian distribution of CNP sizes (Fig. 5C and E) appears not to be reflected in $S(q)$. (iv) The strong interaction regime exhibits a linear regime over 1–2 decades of q with a slope of $D \approx 1.85$–1.88 indicating a fractal structure in Fig. 5C and E. In contrast, the weak interaction regime exhibits no such linear region and, unsurprisingly, the structures of Fig. 5A are not fractal. One might expect that, if the weak interaction case was simulated for a much larger system, then one would obtain a value of $D = 3$ showing that the aggregates formed filled space uniformly, on the average. It can be noted that, if all spheres are atomically identical, as it is in this case of simulating CNPs, then the X-ray scattering, with the background oil subtracted, should look like the curves of Fig. 5B, D and F except for a factor of $|f|^2$, to account for the electron density. We carried out simulations for systems 8 times larger ($L = 100$) and found the same results with the linear portion of Fig. 5D now extending over 2 decades.

It is thus possible to prove theoretically that nanoplatelet aggregation *via* weak attractive dispersion forces together with strong short-range binding will lead to the creation of fractal crystalline aggregates at the mesoscale. It is possible that platelet diffusion under specific interaction regimes is sufficient to explain the fractality in fat crystal networks.

4. Dispersion forces in fats and oils

Fats are soft materials comprising a solid fat crystal network that traps liquid oil.[21,58–61] It is generally believed that the major intermolecular force responsible for maintaining the fat crystal networks (and thus for the solidity of the fat material) is the London–van der Waals dispersion force. The empirical and theoretical implications of van der Waals forces have been

View Article Online

Published on 11 November 2011. Downloaded by Michigan State University on 19/01/2016 06:25:56.

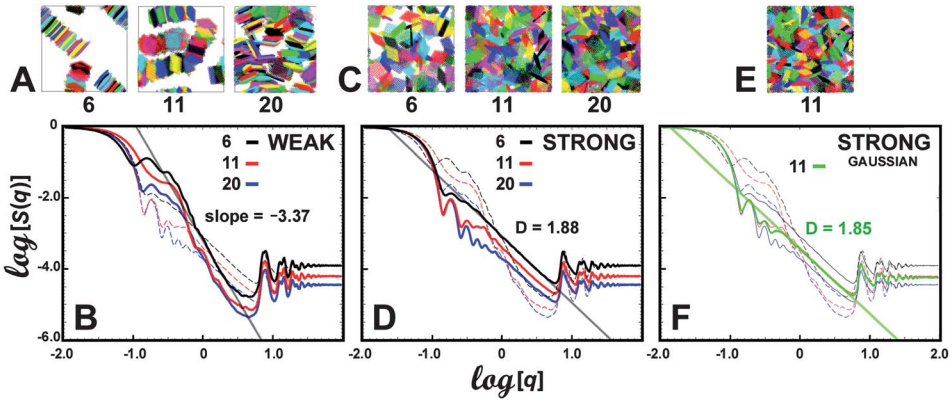

Fig. 5 CNPs at $T = 300$ K. $\log[S(q)]$ *versus* $\log[q]$ for weak (B) and strong (D and F) interactions. (A)–(D) involve CNPs all of the same size, $m = n = 10$. (E) and (F) involve a Gaussian distribution of CNP sizes $\{m \times m \times 1\}$ with average, $\langle m \rangle = 10$, and variance, $\sigma^2 = 5$. The mass concentrations were 6%, 11%, 20% as indicated with black, red and blue respectively for (B and D), and indicated in green for (F). Instantaneous configurations for weak (A) and strong (C and E) interactions. Note that the Bragg peaks possess the same positions in both cases but that the slopes shown in (B) differ from those in (D) and (F).

studied for well over a century. Much of the work has been conducted in colloidal systems, for interfacial energies and for the wetting of surfaces.[52,53,62,63] However, relatively little has been done to study these forces in the context of fat crystal networks. The following section will examine van der Waals forces and their role in the assembly of TAG polycrystalline aggregates.

van der Waals forces arise through the interactions between dipoles. There are three main classes of van der Waals forces—the Keesom force (interactions between two permanent dipoles), the Debye force (interactions between a permanent dipole and an induced dipole) and the London force (interactions between two induced dipoles). London–van der Waals dispersion forces arise through fluctuations in the electromagnetic field. These fluctuations give rise to fluctuations in atomic charge distributions resulting in the formation of fluctuating atomic dipoles. When the internal states of the electromagnetic field are summed up, the result is an effective direct force between the fluctuating atomic dipoles.[63] A key parameter in the theory is the Hamaker coefficient.[64] Much effort has been expended in determining this value. The intent of this section is to provide a brief outline of various approaches used to compute the energy of interaction and the Hamaker coefficient for fats and oils. We shall outline the assumptions made by the various approaches and show that some of these assumptions, although possibly valid at the mesoscale (the scale on which molecular details are "lost"), are invalid at the nanoscale, and discuss alternative approaches.

Interaction energy and the Hamaker coefficient

The system consists of two slabs of nanocrystalline fats (regions 1 and 3) separated by an oil (region 2) shown in Fig. 6.

The slabs possess flat surfaces, an acceptable assumption given the morphology of these crystal platelets, which for simplicity we assume to be parallel. In this scenario, the Hamaker coefficient, A_H, describing the interaction between particles 1 and 3 separated by medium 2 is defined as:[53]

$$U_{123}(d) = -\frac{A_{H123}}{12\pi d^2} \tag{12}$$

The Hamaker coefficient, A_{H123}, is frequently referred to as the "Hamaker constant", a valid description in simple model

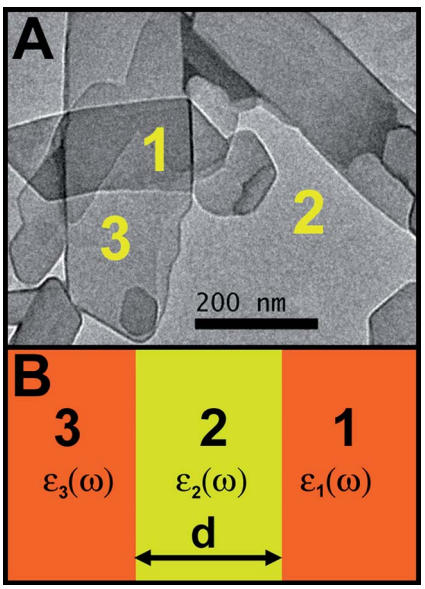

Fig. 6 (A) Crystalline nanoplatelets of tristearin in triolein oil showing two platelets, 1 and 3, and the oil, 2. (B) Schematic diagram of two parallel-faced slabs of crystalline fats, 1 and 3, separated by an oily medium, 2, of thickness d. The permittivities associated with the nanoplatelets are $\varepsilon_1(\omega)$ and $\varepsilon_3(\omega)$, and that of the oil is $\varepsilon_2(\omega)$.

systems.[52] The $1/d^2$ dependence is valid at the mesoscale length scale for certain systems, such as that in Fig. 6, but should not be assumed to be generally valid. In what follows, we will discuss four methods of modeling van der Waals forces in fats systems, noting the significant errors that can arise if one uses, at the nanoscale, approaches valid only at the mesoscale.

Lifshitz theory. Lifshitz theory was developed by E.M. Lifshitz and his co-workers to account for the effect of the dielectric properties of the intervening medium in the system described in Fig. 6 on the van der Waals forces between two particles. This theory considers matter as a dielectric continuum and includes all many-body interactions unlike the classical approach which represents the forces by a sum over only pairwise interactions. However, the assumption of a dielectric continuum results in

 This journal is © The Royal Society of Chemistry 2012

View Article Online

Published on 11 November 2011. Downloaded by Michigan State University on 19/01/2016 06:25:56.

Lifshitz theory being applicable only on the meso- or macro-scale and not at the molecular level. The interaction energies of these phases arise from the electromagnetic field fluctuations which induces fluctuations in atomic electric dipole moments. From the definition of an electrical dipole moment, $\vec{P} = (\varepsilon - \varepsilon_0)\vec{E}$, one can make a plausibility argument that the magnitude of a dipole moment, induced by a fluctuating electrical field, is related to the frequency-dependent permittivity according to $P(\omega) \propto \varepsilon(\omega)$. This yields the Lifshitz expression for the Hamaker coefficient:[52,53,62]

$$A_{\mathrm{H123}} \approx \frac{3}{2} k_{\mathrm{B}} T \sum_{m=0}^{\infty} \Delta_{32}(i\xi_m)\Delta_{12}(i\xi_m) \tag{13}$$

$$\Delta_{ab}(i\xi_m) = \frac{\varepsilon_{ra}(i\xi_m) - \varepsilon_{rb}(i\xi_m)}{\varepsilon_{ra}(i\xi_m) + \varepsilon_{rb}(i\xi_m)} \tag{14}$$

where $\varepsilon_{ra}(\omega)$ is the relative frequency-dependent permittivity for material a ($a = 1, 2, 3$), the sum is over imaginary (Matsubara) frequencies, $i\xi_m$, and the term for $m = 0$ has a prefactor of $^1/_2$. Note the similarity of eqn (14) to an induced dipole expression. In the case that: (1) the permittivities for media 1 and 3 are identical, (2) the permittivities for media 1 and 2 are sufficiently similar and (3) the system responds predominantly only in the UV region, eqn (13) can be approximated by:[53]

$$A_{\mathrm{H121}} = \frac{3}{4} k_{\mathrm{B}} T \left(\frac{\varepsilon_{r1}(0) - \varepsilon_{r2}(0)}{\varepsilon_{r1}(0) + \varepsilon_{r2}(0)}\right)^2 + \frac{3h\nu_{\mathrm{UV}}}{16\sqrt{2}} \frac{\left(n_1^2 - n_2^2\right)^2}{\left(n_1^2 + n_2^2\right)^{3/2}} \tag{15}$$

where n_k ($k = 1, 2$) are the refractive indices of media 1 and 2, ν_{UV} is the electronic frequency in the UV region and h is Planck's constant. Although the original work[63] described spatially homogeneous systems, it can be extended to more complex geometries and spatial dependences,[52] though it is not trivial to treat a system in which the permittivities might be continuously varying functions of spatial position.[62]

The fractal model. From rheological experiments, as well as PLM observations, a model was developed[18,20] that relates the storage modulus, G', to the Hamaker coefficient, A_{H}:

$$A_{\mathrm{H}} = 6\pi a \varepsilon \lambda d_0^2 \tag{16}$$

λ is calculated from the plot of $\ln G'$ with respect to $\ln \phi$[81,82] where ϕ is the solid fraction, a is the diameter of a fat primary crystal, ε is the extensional strain at the limit of linearity and d_0 identifies the equilibrium distance between the flocs. For the case of tristearin in triolein oil,[65] $\lambda = 1.17 \times 10^7$ Pa, $\varepsilon = 1.9 \times 10^{-4}$ and $a \approx 150$ nm.[35] However, the value of d_0 is unknown.

The semi-classical model. The semi-classical model relates the Hamaker coefficient A_{H} to the disjoining free energy of a fat crystal[66] separated into two blocks at their equilibrium separation, d_{e}:

$$A_{\mathrm{H}} = 24\pi\gamma d_{\mathrm{e}} \tag{17}$$

where γ is the interfacial free energy per unit area. As in the fractal model, the value of d_{e} is unknown.

From eqn (16) and (17) we have two unknowns: the equilibrium distance between flocs, d_0 and the equilibrium distance between two blocks of fat crystals, d_{e}. For eqn (15), we must know the values of $\varepsilon_{ri}(0)$ and n_i, the static permittivity and refractive index for both the solid fat ($i = 1$) and the oil ($i = 2$). Although these values are measurable in a macroscopic (millimetre-scale or larger) system, it is not obvious that those values can be used when the two slabs are separated by mere nanometres.

The Lennard-Jones (L-J) 6–12 potential. The Lennard-Jones (L-J) 6–12 potential, $u_{AB}(r)$, describing the London–van der Waals energy of interaction between two spherically symmetric atomic moieties, A and B, is,[53]

$$u_{\mathrm{AB}}(r) = -\frac{C_6^{\mathrm{AB}}}{r^6} + \frac{C_{12}^{\mathrm{AB}}}{r^{12}} \tag{18}$$

where we have denoted the energy between two atomic moieties, the smallest objects that go to make up larger systems, by a lower-case u. Here r is the center-to-center distance between A and B. While the attractive $1/r^6$ term can be justified from first principles, the form of the repulsive, $1/r^{12}$ term, representing the electron "overlap" repulsion between different atoms, has been chosen for computational convenience. Eqn (18) is also used to represent the interaction energy between two infinitesimal "chunks of matter" and has been utilized in Mean-Field theories other than those described above.[53]

If one knows the functional form of the number densities, $\Phi_i(\vec{r})$, of the solids ($i = 1, 3$) and the oil ($i = 2$), then one can use the Lennard-Jones 6–12 potential to compute the total energy of the system and, from it, deduce the Hamaker coefficient. The energy of the system of Fig. 6B interacting *via* the 6–12 potential is:[52,53]

$$U_{123} = \sum_{j \neq i} \int_i d^3\vec{r} \int_j d^3\vec{r}' \left[\frac{-C_6^{ij}}{\left|\vec{r} - \vec{r}'\right|^6} + \frac{C_{12}^{ij}}{\left|\vec{r} - \vec{r}^{ij}\right|^{12}}\right] \Phi_i(\vec{r})\Phi_j(\vec{r}') \tag{19}$$

where the sum is over $i, j = 1, 2, 3, j \neq i$ and the double-counting of energies is disallowed. The coefficients, C_n, describe the interaction energy ($n = 6, 12$) between substances i and j. One has to make some assumptions about the number densities and the most common assumption is that they are constant, independent of the nanoplatelet separation, d. However, if one requires that the chemical potential (free energy per molecule) of the slabs in Fig. 6B is equal to the chemical potential of a pure-oil system (the "bulk") in contact with the slab system, then one need not assume that the number densities are constant. From this, one can obtain an average number density of oil between the two nanocrystals as a function of d.

Atomic scale molecular dynamics. Atomic scale molecular dynamics is probably the best technique to study the structure and dynamics of fats and oils at the nanoscale. Many modeling studies have been carried out on triacylglyceride (TAG) systems.[67–70] An open problem is to model the condensation of TAG molecules into a crystal and the identification of the various polymorphic forms. We carried out simulations in order to see to what extent the assumption that the liquid oil was homogeneous when the distance, d, (Fig. 6) was a few

View Article Online

Published on 11 November 2011. Downloaded by Michigan State University on 19/01/2016 06:25:56.

nanometres. We modeled the radial interactions between 'non-bonded' TAG atomic moieties using GROMACS, an atomic scale molecular dynamics simulation package.[71,72] TAGs possess only CH, CH_2, CH_3, O and C=O moieties and the GROMACS manual[54] lists the GROMACS coefficients (C_6 and C_{12}) which define the L-J potential between given pairs of these atomic moieties. One must make a decision as to which ensemble to use and it might appear that the *NpT* ensemble (constant number of molecules, pressure and temperature) is the "natural" one. However, the strength of computer simulation is that one can create systems that are not found in the lab, allowing other ensembles to be easily studied. Our model should describe a system comprising two fats particles immersed in a bulk TAG fluid in the *NpT* ensemble, so that the TAG molecules can explore all of space. This scenario is not practicable and, instead, we represented the bulk and the fats particles (Fig. 6) separately and required that the chemical potential of the fats particles system to be equal to that of the bulk. We represented the fats particles as tristearin nanocrystals and the oil as triolein. Because we know the density of a bulk triolein fluid, ~930 kg m^{-3}, we used the *NVT* (constant number of molecules, volume and temperature) ensemble for both the bulk and the system of Fig. 6 with periodic boundary conditions in the planes perpendicular to the interfaces. Here, molecular dynamics simulations were performed using GROMACS in *NVT* ensembles with periodic boundary conditions employing the force field given by Berger *et al.*[73] and using the V-rescaled thermostat. The solids were represented as continua interacting with each other by replacing the individual molecules by average values of the Lennard-Jones parameters and using eqn (19). The coefficients, C_6 and C_{12} ($i, j =$ 1, 2), were replaced by their averages over the atomic moieties making up the solids. Similarly, the interactions between the crystalline solids and the atomic moieties of the liquid TAGs, eqn (18), were represented by Lennard-Jones parameters, C_6 and C_{12}, averaged over the atomic moieties, A, making up the solid. These interactions between the average solid atomic moiety and oil atomic components were used in the molecular dynamics simulation. Finally, eqn (18) can be used to describe the interactions within the oil with no averaging used.

The utility of Lifshitz theory to understand interactions and structures in food components. Eqn (15) has been used for fats and oil systems. Johansson and Bergenståhl[74] used tristearin for regions 1 and 3 (Fig. 6) and soybean oil for region 2 using tabulated refractive indexes and dielectric permittivities. Kloek[75] calculated the Hamaker coefficient for the same system, using a slightly different refractive index than Johansson. Their results showed that a slight variation in the value of the permittivity resulted in Hamaker coefficients differing by a factor of ~10.

We calculated the Hamaker coefficient using the four continuum approaches described here. The system for which the calculation was conducted was a mix of fully hydrogenated canola oil (regions 1 and 3) and high oleic sunflower oil (region 2) at 30 °C.[44] For mesoscopic systems, it is essential that the frequency-dependent relative permittivity, in particular the static permittivity, $\varepsilon_r(0)$, be measured accurately since seemingly small errors can give rise to large errors in the Hamaker coefficient, A_H. Using the approximate Lifshitz theory (eqn (15)) and experimental values for $\varepsilon_{r1}(0)$ and $\varepsilon_{r2}(0)$, n_1 and n_2, the calculated Hamaker constant A_H was approximately 0.44×10^{-21} J. Using GROMACS, we estimated the value of the averaged attractive parameter to be $\langle C_6 \rangle = 1.183 \times 10^{-23}$ J nm^6. Since both the fluid and the solids possess acyl chains with 18 carbons, we may use this value for both the fluid triolein and the solid nanoparticles. The only difference then is the density of the solid and the fluid. Using our measurements for densities and number densities, we obtained a value for the Hamaker coefficient of the continuum L-J 6–12 potential theory of $A_H = 3.53 \times 10^{-21}$ J. Note that the value of d_0, the distance at which the energy is a minimum, is $d_0 =$ 0.275 nm. For this value of d there can be no oil between the nanoparticles. By equating $d_0 = d_e$, and using the value of $d_0 =$ 1.5 nm obtained from the ASMD simulation, we calculated values of the Hamaker coefficients, A_H, for the fractal and semi-classical models. We obtained $A_H = 14.1 \times 10^{-21}$ J for the fractal model and $A_H = 880 \times 10^{-21}$ J for the semi-classical model. If, however, we used the value of $d_0 = 0.275$ nm, we would obtain $A_H = 0.47 \times 10^{-21}$ J for the fractal model and $A_H = 28.5 \times 10^{-21}$ J for the semi-classical model. These are Hamaker coefficients when there is no oil between the nanoplatelets.

We thus obtained a wide range of values for A_H all in units of 10^{-21} J: (i) from Lifshitz theory we obtained 0.44; (ii) we obtained 3.53 (continuum Lennard-Jones model for which $d_0 = 0.275$ nm); (iii) with $d_0 = 1.5$ nm, we obtained 14.1 (fractal model) and 880 (semi-classical model).

To further evaluate the utility of Lifshitz theory on the nanoscale, we computed the average oil number density, $\langle \Phi(d) \rangle$, between the slabs as a function of slab separation, d. We found that this quantity exhibited a decrease of up to ~50% between the slabs as d decreased with $d \geq 1$ nm. Similar observations have also been made in simulations of van der Waals spheres and hard spheres in nanotubes.[76,77] What our results show is that, when two fat particles are separated by a few nanometres, the oil between them can be expelled. The effect of this is to invalidate the assumption that the van der Waals energy of interaction between the two slabs of Fig. 6 exhibits a $1/d^2$ dependence with a constant Hamaker coefficient. Our analytical calculations on a model system showed that the van der Waals energy density possessed terms in $1/d$, $1/d^2$, and $1/d^3$. Of course one can always define a d-dependent Hamaker coefficient but this rather defeats the purpose of this quantity. Accordingly, the utility of the elegant Lifshitz theory can be questioned on the nanoscale: what value of permittivity does one insert into eqn (13) and (15) when the oil exhibits density changes on a length-scale of ~0.5 nm?[78]

Our computer simulation results showed that one cannot blithely use Mean Field theories to characterize oils trapped between two fats surfaces when the latter are sufficiently close together. It may be, however, just this region, where the solid fats are ~1 to 2 nm apart, which is ultimately responsible for the mechanical properties of TAG systems. One might use multi-layered models as described by Parsegian,[52] to approximate the oscillatory liquid density but, in order to discover the characteristics of the oscillations, one must carry out the computer simulation done here. However, since the entire problem would then have been solved, it would be unnecessary to use Mean Field theories. Accordingly, when investigating the physical properties of oils in confined spaces, it is prudent to employ atomic scale molecular dynamics.

 This journal is © The Royal Society of Chemistry 2012

View Article Online

Published on 11 November 2011. Downloaded by Michigan State University on 19/01/2016 06:25:56.

5. The link between microstructure and mechanical properties

For most semisolid fat products, textural properties are determined by the solid component of the system, which normally exists as a 3-dimensional colloidal fat crystal network. Similar to colloidal gels, fat crystals aggregate during crystallization and grow into clusters, flocs and finally a network of these flocs. An illustration of a fat crystal network at different length scales is shown in Fig. 1. This structural hierarchy within fat crystal networks has been recognized by many groups.[4,60,79,80] Refinements to this structural hierarchy were further developed during later work involving the modeling of the rheological properties of fats.[18,81] Fig. 1 shows an illustration of the structural hierarchy in fat crystal networks.

Of great interest from both an applied and theoretical perspective is the influence of the microstructure on the macrophysical properties (particularly mechanical strength) of a fat material. For example, the shear elastic modulus G (a suitable indicator of the hardness of a fat) obtained from small deformation rheological measurements has been found to be sensitive to the microstructure of fats.[82] While many empirical correlations between structural parameters (such as the crystal aggregate size) and the mechanical properties (such as hardness) of fats are known, much less is known about their relationships in terms of mechanisms.

It is obvious that the storage modulus, G', or other rheological measures of solidity, cannot be simply related to the molecular structure or composition of the triacylglycerol molecules which make up a fat material. The rheological properties of fats are a result of the combined effect of the solid fat content (SFC) and the microstructure of the fat crystal networks, including the shape, size and spatial distribution pattern of the fat crystals.[3,58,59,83,84] In order to fully understand and eventually predict the macroscopic properties of these soft, plastic materials, it is necessary to characterize and define the different levels of structure present and their respective relationships to the mechanical properties of fat.[85] From the 1960s onwards, many attempts have been made to elucidate the relationship between the elastic modulus of colloidal networks and their structural characteristics but only a few of them have been partially successful.[58,81,86]

The linear chain model and modified linear chain model

The first model used in the study of colloidal fat crystal networks was the linear chain model, which was proposed by van den Tempel in 1961.[58] In this model, a fat was described as a colloidal material composed of flocculated crystals of colloidal dimensions embedded in a liquid phase. In this model, a 3-dimensional network of solid particles is formed by aggregation of the dispersed particles and it is this network that is responsible for the elastic nature of the system. Van den Tempel proposed that solid fat crystals are held together by two types of bonds—irreversible primary bonds and reversible secondary bonds. Solid fat crystals interacting *via* these forces will form linear chains and then these chains eventually form a fat crystal network. The primary bonds are stronger than the secondary bonds and may consist of relatively strong van der Waals interactions. The breakage of strong irreversible primary bonds was used to explain the work-softening phenomenon observed in margarine and butter after kneading.[59,79] In this model, the shear modulus, G, is predicted to scale linearly to the volume fraction of solids, Φ, according to eqn (20):

$$G = \frac{5A\Phi a^{0.5}}{24\pi H_0^{3.5}} \tag{20}$$

where A is Hamaker's constant, H_0 is the interparticle distance and a is the particle size. This model was developed for particles with a geometry between that of a sphere and that of a cube. However, experimental results showed that the elastic shear modulus of fat samples, G, does not scale linearly with the solids volume fraction Φ. This does not agree with predictions from the linear chain model. Instead, G increases in a power-law fashion relative to the solids volume fraction.[4,59,81,87,88]

Realizing the deficiencies of the linear chain model, several researchers tried to modify the model by introducing an intermediate level of structure between the primary fat crystals and the infinite network. For example, in Sherman's model,[86] colloidal fat crystal networks were described as less-densely-packed areas formed by the joining of localized regions of densely packed particles. Van den Tempel also realized that an intermediate level of structure[60] was indeed necessary to explain the rheological properties of fats and he proposed an "extended" linear chain model. In this model, the chains consisted of crystal aggregates instead of individual spherical fat crystals. The interaction between neighboring aggregates in a chain was proposed to be the sum of the interactions between the particles in contact between aggregates. The tensile force in one principal direction was related to the interaction between particles in contact. A correction factor was introduced in the calculation of the shear modulus of the fat crystal networks. The shear modulus, G, was recalculated as:

$$G = G_{\text{theory}}\frac{nD_{\text{a}}}{Na} \tag{21}$$

where G is the corrected shear modulus of fat crystal networks, G_{theory} is the shear modulus of the networks calculated from the linear chain model, n is the number of the connecting chains between two neighboring aggregates, N is the average number of primary particles in an aggregate, D_{a} is the average diameter of an aggregate, and a is the average primary particle diameter. The complete formula of the modified linear chain model is:

$$G = \frac{5A\Phi nD_{\text{a}}}{24\pi H_0^{3.5}a^{0.5}N} \tag{22}$$

Although the modified model fitted the experimental results better than the original model, the question remains as to whether there is a mechanistic explanation underpinning the correction factor or whether it is just an empirical value to allow a better fit of the data to the model. It is almost impossible to independently find values to calculate the correction factor. Moreover, the scaling behavior between the elastic modulus and the solid fat content was still not successfully explained. Therefore, the modified linear chain model has not been widely adopted.

View Article Online

Published on 11 November 2011. Downloaded by Michigan State University on 19/01/2016 06:25:56.

The fractal model

The self-similar character of fat crystal networks observed by Narine and Marangoni[18] led us to propose that the geometry of fat crystal networks can be considered to be fractal. The fractal dimension can then be determined *via* several methods including rheology, microscopy, oil migration, and light scattering.[89,90] Fractal dimensions calculated by different methods are sensitive to different structural features of the fat crystal network. For example, realizing that the number of particles of the object, N, has a power-law relationship to the length scale, L, *i.e.*, $N \approx L^D$, the particle-counting fractal dimension of the fat crystal networks can be derived from the exponential term of this power law relationship. Fractal dimensions calculated by microscopy methods such as box-counting, particle-counting, and Fourier Transforms of polarized light micrographs of fats have been used to quantify the microstructure of fat crystal networks.[84,91] The fractal dimensions describe the combined effects of morphology and spatial distribution patterns of the fat crystal clusters in the fat crystal networks.[92]

In the study on the rheological properties of colloidal gel networks, Shih and others considered a 3-dimensional colloidal network as being composed of inter-connected flocs and the fractal dimension was used to quantify the relationship between the average floc size and the particle concentration of the colloidal network.[93] Based on the relative value of the elastic constant of the interfloc links to that of the flocs, two regimes were identified, the strong link regime, where the elastic constant of the interfloc links is larger than that of the flocs, and weak link regime, where the elastic constant of the interfloc links is smaller than that of the flocs.

Vreeker and others realized the fractal nature of fat crystal networks and explained the power law relationship between the G' and solid fat content (SFC) data for fat samples with low solid fat content (<10%) using Shih and others' strong-link regime.[94] The fractal dimension of the networks was determined using a light scattering method.

Work conducted by our laboratories has shown that fat crystal networks at high solid fat contents behave rheologically as if they were in the weak-link regime.[18,20,81,85] In the studies on the microstructure and the rheological properties of fat crystal networks, the interfloc links of the network have been found to carry most of the stress loaded on the system and both the elastic constant and the limit of linearity increase with increasing particle concentration.[21,79,81,84,95] Thus, fat crystal networks have been proposed to be in the weak-link regime.

By combining the weak-link regime theory and fractal geometry, a fractal model of fat crystal networks has been proposed. Marangoni further developed the fractal model of the fat crystal networks and extended it to more general colloidal networks using a thermodynamic approach.[20] A general expression for the relationship between the elastic modulus and the microstructure of high volume fraction aggregate networks has been obtained:

$$E \approx \frac{12\left(\frac{\Delta U_\xi}{(l_0 - l)}\right)}{\pi a \xi \varepsilon} \Phi^{1/(d-D)} \tag{23}$$

where E is the Young's modulus of the fat crystal networks, ΔU_ξ corresponds to the change in the internal energy per floc–floc bond, l_0 is the effective distance between flocs, l corresponds to the distance between flocs under an applied stress, a is the diameter of the particles within a floc, ξ is the diameter of the flocs, ε is the compressive strain of the network ($\varepsilon = \Delta L/L$, where ΔL is the deformation of the network and L is the size of the network), Φ is the volume fraction of the aggregates of the network (Φ = SFC/100), d is the Euclidean dimension of the embedding space, and D is the fractal dimension for the arrangement of particles within the network. By substituting ΔU_ξ with interparticle interaction energy in a specific network, this extended model is suitable to study any soft material structured as a particle network at high volume fractions. For example, if the interaction forces between the structural elements of a fat crystal network are purely van der Waals, the Young's modulus, E_s, and the shear modulus, G_s, of a fat structured as a space-filling collection of spherical crystal clusters are:

$$E_s \approx \frac{A}{2\pi a \varepsilon l_0^2} \Phi^{1/(d-D)} \tag{24}$$

$$G_s \approx \frac{A}{6\pi a \varepsilon l_0^2} \Phi^{1/(d-D)} \tag{25}$$

This model has been extended to the study of the yield stress of soft materials.[21] An expression of the yield stress of a fat was obtained:

$$\sigma^* \approx \frac{6\gamma}{a} \Phi^{1/(d-D)} \tag{26}$$

where σ^* is the yield stress, γ is the solid–liquid surface energy (or the crystal-melt interfacial tension). The yield stress as a function of solid's volume fraction for blends of milk fat, cocoa butter, and modified palm oil have been studied by small deformation rheology experiments. The results agreed well with the model described by eqn (26).

The fractal model explains the elastic properties of fat crystal networks by the summed stiffness of the inter-floc links. The increase of G' with SFC has been explained by the increase in the number of inter-floc links with SFC. In the fractal model, the fractal dimension of fat crystal networks has been assumed to remain unchanged within certain SFC ranges; however, Awad and others showed different fractal dimensions in different SFC ranges for the same fat sample.[95] This could have arisen due to changing growth/aggregation modes at different volume fractions of solids. As explained in Section 3, changes in aggregations modes can lead to the formation of very different structures—even to the extent that the structure is not fractal any longer. Ultimately, this would arise due to changes in the medium's viscosity and possibly in the strength of van der Waal's forces between nanoplatelets.

Heterogeneous stress distribution and the modified fractal model

The idea of a heterogeneous stress energy distribution has been accepted in the field of statistical mechanics for a long time. When a colloidal network is stressed, a small part of the material carries most of the stress, while the other part of the material contributes very little to the elastic properties of the material. This idea comes from the fact that there are always imperfections in the structure of materials.

 This journal is © The Royal Society of Chemistry 2012

View Article Online

Published on 11 November 2011. Downloaded by Michigan State University on 19/01/2016 06:25:56.

As early as in the 1920s, Griffith realized that the true value of the strength of some materials was as much as 1000 times less than their theoretical strength.[96] He discovered that there are many microscopic cracks in every material, which were present at all times. He hypothesized that these small cracks actually lower the overall strength of the material because stress applied on the material is concentrated at the crack tips, where a stress concentration is experienced. It should be noted that not only the microscopic cracks can act as stress concentrators, but also any voids in the material, corners, and hollow areas within the material can also act as stress concentrators and lower the overall strength of the material.

For many colloidal networks, the system is composed of interconnected structural clusters with hollow spaces in between. The hollow space of largest size in a region represents a kind of "flaw" and becomes a stress concentrator in that area. The elastic properties of the whole network, in fact, are dominated by the elastic strength of these stress concentrators. This hypothesis has been proven by many experimental results.

For example, during the studies on aerogels, Woignier and Despetis found that the strength of the gel strongly depended on the presence of flaws.[97] Failure was assumed to be a result of stress concentration at the flaw tip. When stressed, the strength of the gel is characterized by a given value of the stress intensity factor K_I, which is related to the applied stress and the flaw dimension. Failure occurs when K_I reaches a specific value K_{Ic}. Through simulation, Beale showed that the failure stress of materials is determined by the linear dimension of the critical defect, which is a function of the system linear size and the largest defect size.[98] Even for some seemingly perfect networks, due to the differences between the structural clusters, the stress distribution is still heterogeneous. In a numerical study on sheared monodisperse (uniform grain size) and polydisperse (heterogeneous grain size) granular networks, Bardenhagen and Brackbill showed that an exponential probability distribution of the principal stress difference within granular materials was found to be independent of the type of loading, grain size distribution, and the packing fashion.[99] This appears to be a characteristic of the heterogeneous nature of the load-carrying mechanism in granular materials.

In a fat crystal network, crystal flocs are not uniform. The shape, size, and strength of the fat crystal flocs making up the fat crystal network are always polydisperse. The weakest floc will become a flaw and thus act as a stress concentrator. Thus, the stress distribution between fat crystal flocs in a fat crystal network is also heterogeneous. Kloek and others noticed that the fracture of fat crystal networks under large deformation is initiated at a defect or inhomogeneity during their compression in wire-cutting experiments on dispersions of fully hydrogenated palm oil in sunflower oil with varying fractions of solid fat.[100] A combination of the energy input from compression experiments and the specific fracture energies from wire-cutting experiments yielded defect lengths of the order of 20 μm, which corresponds to the size of a fat crystal aggregate at the start of solidification.

In addition to the effects of flaws, the connectivity also plays an important role in the heterogeneous stress distribution within colloidal networks.[101,102] A number of studies have shown that the elastic modulus of colloidal networks shows a power-law dependence on their relative density.[20,103–105] For fully connected networks and foams, computer simulation studies demonstrated that the modulus of the networks was proportional to the square of the density;[106] however, higher exponents have also been observed in experiments and have been attributed to the presence of dangling ends,[107] which is the mass not included in the 3D network.

Due to the existence of these "dangling ends", some solids or solid clusters do not have a connection with neighboring clusters or are only connected to one of the neighboring clusters, and are thus not included in the network and contribute nothing to the elastic properties of the material. Thus, the elastic properties of the network depend on the number of connections between neighboring structural clusters, rather than on the amount of apparent solids. An increased connectivity leads to a higher value of the elastic modulus of the material as what was observed by Duffours and others during their studies on the bulk modulus of aerogels before and after compression.[101] The bulk modulus of aerogels increased after compression. The bulk modulus of the aerogel with a low initial concentration of solids was found to increase faster than that of aerogels with high initial concentration of solids, although the absolute value of the first ones were still smaller than that of the last one. The increase in modulus was explained by increased network connectivity. This implies that the connectivity of the networks increases with increasing volume fractions of solids.

This idea was further explored in the Finite Element Analysis (FEA) study conducted by Ma and others.[108] The networks used in the simulation were created by diffusion limited cluster–cluster aggregation (DLA), and a fully connected network was obtained when all clusters were connected to at least two neighboring clusters. The bulk modulus of the original networks was much lower than that of the corresponding fully connected networks at low bulk density; however, at high bulk density, the bulk modulus of both networks became similar, implying the original networks became more and more fully connected at higher bulk densities. Furthermore, the simulation also showed that even for a "perfectly connected" network, there was still an abundance of unloaded bonds. Still, however, the load-carrying bonds were concentrated in the more open spaces, which is consistent with Griffith's theory on stress concentration along flaws. Moreover, the volume fraction of the load-bearing solids within the networks was found to increase in a power-law fashion with the apparent volume fraction of solids for a fully connected network. Considering that real networks are not fully connected, and that connectivity of networks increases with the volume fraction of solids, it is possible that the load-bearing volume fraction of solids in real networks increases in an exponential fashion with the apparent volume fraction of solids. The load-bearing volume fraction is always less than the apparent volume fraction of solids of the network, and it becomes closer to the apparent volume fraction of solids at higher volume fractions.

Based on the principle of heterogeneity in stress distribution and network connectivity, Tang and Marangoni[109] used a probabilistic approach to derive an expression for the effective volume fraction of solids, Φ_e, namely:

$$\Phi_e = 1 - e^{-k\Phi b} \tag{27}$$

where k and b are constants. Thus, the elastic properties of colloidal networks are dependent on the load-bearing volume

View Article Online

Published on 11 November 2011. Downloaded by Michigan State University on 19/01/2016 06:25:56.

fraction of solids, which is an exponential function of the apparent volume fraction of solids. Replacing the SFC of a fat crystal network, Φ, in the formula of the Young's modulus for fat crystal networks ($E_s \approx (A/2\pi a\varepsilon l_0^2)\Phi^{1/(d-D)}$, eqn (24)) by the expression of Φ_e, an expression for the Young's modulus of fat crystal networks for the modified fractal model is obtained:

$$E \approx \frac{A}{2\pi a\varepsilon l_0^2}\left(1 - e^{-k\Phi^b}\right)^{1/(3-D)} \quad (28)$$

This modified fractal model distinguishes between the effects of network microstructure and the effects of heterogeneous stress distribution and network connectivity.

6. Engineering crystalline structure using external fields

The heat, mass and momentum transfer conditions imposed during the formation of a fat crystal network have significant effects on the final microstructure and macrophysical properties of fats. A field can be described as a spatial distribution of a physical variable (such as temperature or velocity) within a given volume. During crystallization, one could define as many fields as there are variables that take a local value within the volume being crystallized. In the simplest case, the fields can be described by scalar (temperature) or vectorial (velocity) entities, though in the case of rheological behavior it is often necessary to use tensors for this description.[110,111] As has been explained earlier, the main driving force for crystallization of triglycerides is a difference between the chemical potential of each component in liquid and the chemical potential of the same component in the solid phases to be formed.[112] This difference in the chemical potential is mostly the result of the temperature difference between the saturation temperature of the liquid and the temperature of crystallization. Thus the most important field in crystallization is the temperature field. There are several other conditions that can affect the crystallization at a given location: a spatial distribution of heterogeneous nucleation sites; a concentration field;[113,114] a distribution of velocities resulting in a shear rate field;[115,116] an applied ultrasound field;[117,118] the presence of magnetic[119,120] or electric fields;[121] a pressure field and the ubiquitous gravitational field.[122] We will focus our review and discussion on temperature, concentration and shear flow fields since they are the ones that are currently most relevant to fat crystallization. The temperature, concentration and shear fields are interrelated by the momentum, heat and mass transport mechanisms in the material.[110]

Temperature gradients

In the case of temperature, it is very common in scientific research to assume that the whole sample is under isothermal conditions. At a macroscopic level, this is likely the case for experiments performed on thin layers of material (as is the case for many static microscopy studies) where the transfer of heat can be considered to occur almost instantaneously.[123] This condition becomes somewhat more difficult to achieve in larger "bulk" samples.

A low thermal diffusivity will tend to produce a large gradient in the temperature field during heat transfer processes. Crystallization is, by its very nature, a transient process. The low thermal diffusivity will produce high thermal gradients when very fast cooling rates are expected, or when large amounts of crystallization heat need to be removed. When the material is cooled quiescently, some natural convection and movement are still possible. This would tend to mitigate the established gradient. However, the presence of thermal gradients is unavoidable. This means that there will be a gradient of crystallization conditions in the material, and therefore a gradient of crystalline properties.[113] It is therefore not surprising that results for rather large static samples do not correlate well with smaller samples. Typical studies of 'large samples' include large mixing systems,[124] common 10 mm NMR tubes,[125] round pucks,[17] *etc.* An intermediate size is often used in capillary holders.[32,126] Relatively small samples are used in differential scanning calorimetry (typically 10 mg) studies and in microscopy (10–50 μm sample thickness).

To gain a better perspective on the effect of thermal gradients as a function of sample sizes, it is useful to consider the thermal properties of fats. Unfortunately, there is a general lack of physical and physico-chemical data on triglycerides and their mixtures, especially in the solid state. Part of this is due to the complexity of their polymorphic behavior, as discussed earlier. Another issue is that they form solid solutions and multiphase systems. Even with the same polymorphic form, they can have co-existing solid phases of different compositions. Available data suggest a thermal conductivity of roughly 0.16 to 0.18 W $(m \cdot °C)^{-1}$ for molten fat.[127–129] The specific heat of molten fat is about 2 kJ $(kg\ °C)^{-1}$.[130] With a typical density of around 900 kg m^{-3}, the thermal diffusivity of fat melts is in the order of 10^{-8} m^2 s^{-1}. Upon crystallization, the density may increase up by about 10%[131] whereas the specific heat decreases.[132] The thermal conductivity is expected to increase although data attesting to this is scarce. The thermal properties of solid triglycerides depend on the polymorphism and composition of the solid phase. If the thermal properties of triglycerides are similar to those of hydrocarbons[133] the thermal conductivity of solid triglycerides is 2.7 times the thermal conductivity of the molten state. This gives a value of around 0.49 W $(m\ °C)^{-1}$.[134] The time it would take for the centre of a cylinder of liquid fat with a diameter of 9 mm (typical NMR tube) to cool down from 70 °C to 10.1 °C (in the absence of convection), after being immersed in a 10 °C bath would be 40 min. This is assuming the absence of phase transformations. In the event of a phase transformation such as crystallization, the time necessary for the above-mentioned decrease will be longer than 40 min as the heat of crystallization needs to be removed. For a 1.5 mm capillary, the same temperature decrease can be achieved in about 67 seconds.[135] The times for a solid triglyceride would be 15 min (9 mm tube) and 22 seconds (1.5 mm capillary). The changing temperature gradients and local temperature-time histories will therefore produce a somewhat heterogeneous material, especially when the original material is a multi-component mixture of triglycerides. There is a need for the application of more accurate cooling models to explain the results obtained using different techniques.

Concentration fields

As soon as crystallization starts, a concentration field will be established in the liquid phase, since the components that tend to

 This journal is © The Royal Society of Chemistry 2012

View Article Online

Published on 11 November 2011. Downloaded by Michigan State University on 19/01/2016 06:25:56.

crystallize more readily will be depleted faster from the solid–liquid interface than those that tend to crystallize less readily. Thus, a transient field exists at the moving solid–liquid interface.[136] The concentration field can be allowed to develop spontaneously under static conditions, or it can be modified externally. The modification can be achieved by a combination of mechanical operations that include mixing and separation of the liquid and solid phases. This is frequently carried out in dry fractionation. Controlling the concentration profiles allows for some control of the crystalline compositions obtained.[137–139]

Shear fields

The most common external field (after temperature) used to engineer crystallizing fats is the flow field. This field is normally an ill-defined combination of extensional and shear flows.[140] Typical industrial scraped-surface heat exchange units such as Votators™ apply high shear rates near the heat-exchange surface. The flow pattern throughout the rest of the unit is more or less turbulent. Experience within the fat processing industry has shown that the tempering of fats is expedited by the application of shear flow.[141] Detailed rheological data on this effect have been obtained for cocoa butter and possible mechanisms have been proposed.[142–144] Based on the empirical lore and detailed scientific studies, it was clear that the application of a shear field dramatically reduced the time needed for cocoa butter to transform to the polymorphic form V (β) from the metastable phase(s) initially obtained during the beginning of crystallization. Studies on sheared chocolate showed the same effect.[45,145–147] The first direct observation of the accelerated phase transformations in sheared cocoa butter was reported in 2002 from data obtained using synchrotron X-ray diffraction.[148] The effect of shear on the kinetics of polymorphic transformations was later shown to be universal.[33]

In recent years, there have been several studies on the effect of a shear flow field on the crystallization of different fat systems. Analysis of the X-ray diffraction patterns of fats crystallized under shear indicated that the fat crystals were oriented when high shear rates were applied. The 3D structure of the aligned layers of crystalline particles in a fat material was illustrated by Maleky *et al.* (Fig. 7). This figure clearly shows that laminar shear applied in a Couette-type device can promote the orientation of crystallites in a direction parallel to the shear field. As shown in Fig. 7B, the alignment effect is absent if the crystallites are merely "mixed" as occurs in the shearing of the melt in a beaker.

The fat crystals had thicknesses between 30 and 120 nm. It was suggested by Mazzanti and others[33] that the constitutive units of the crystalline network were not the micrometre-sized "crystals" observed in most published micrographs. The platelets would have a thickness ξ around 100 nm according to the corresponding X-ray diffraction peak. This thickness was calculated using an approximation of the Scherrer formula for small angle X-ray diffraction,[149] as mentioned earlier:

$$\xi = \frac{2\pi}{\Delta q} \tag{29}$$

Δq is the full width at half maximum of the small angle X-ray diffraction peak produced by a given solid phase, in coordinates of the scattering vector $\boldsymbol{q}$ defined as $\boldsymbol{q} = 2\pi/d$ in nm^{-1}.

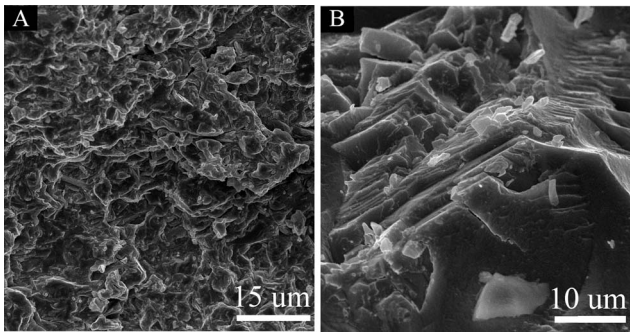

Fig. 7 Cryo-SEM micrographs of cocoa butter crystallized under various shearing conditions. (A) Randomly oriented cocoa butter crystals formed by agitating the melt with a mixer (shear-mixed). (B) Oriented cocoa butter crystals formed by laminar shearing of the melt in a Couette-type device.

The likelihood of the platelet hypothesis was strongly reinforced by the results of recent experiments.[150–155] The discovery of crystalline nanoplatelets *via* electron microscopy by Acevedo and Marangoni in 2010 finally proved the proposed hypothesis.

The observed orientation also indicated that the applied shear flow had an effect on the aggregation of the crystalline nanoplatelets. The fraction of "free" to "aggregated" nanoplatelets depended on the shearing conditions. Higher shear rates increased the fraction of "free" platelets, yielding a more oriented diffraction pattern. Static or very low shear rates favoured the aggregation of platelets, thanks to the colloidal attractive forces described in earlier sections. These "clusters" of platelets do not result in a diffraction pattern characteristic of oriented crystals as the aggregation process results in the random orientation of the nanoplatelets. This can be observed in Fig. 8, which shows two diffraction patterns of a mixture of pure triglycerides crystallized in the presence (A) or absence (B) of shear flow. This highlights even more the importance of the modeling studies of NCP discussed in Section 2 of this review.

The recent advances in the understanding of the nanostructure of fats have changed the paradigm on fat crystallization processes. This has significant theoretical and technological implications, for instance on chocolate manufacture. Chocolate is a "decadent" fat product of high added-value whose main fat ingredient is cocoa butter. Given this strong economic incentive, it is not surprising that many recent papers have dealt with the crystallization of cocoa butter under shear flow.[156] In a few instances, work on the effect of shear on chocolate itself (considerably a more complicated system that just cocoa butter) has been conducted.[157–160]

In the work of MacMillan and others,[148] it was observed that cocoa butter went directly from a metastable phase (initially thought of as form III, a type of β′ polymorph) to the stable and desirable form V (a β polymorph) without going through phase IV as it usually does under static conditions. No orientation was observed at their highest shear rate of 12 s^{-1}, but a reduction in the onset time for the transition to form V was observed. The studies conducted by Mazzanti and others broadened the range of conditions, reaching shear rates as high as 2880 s^{-1}.[33,151] It was shown that the phase-path followed by the crystallization process depended on a combination of the crystallization temperature

View Article Online

Published on 11 November 2011. Downloaded by Michigan State University on 19/01/2016 06:25:56.

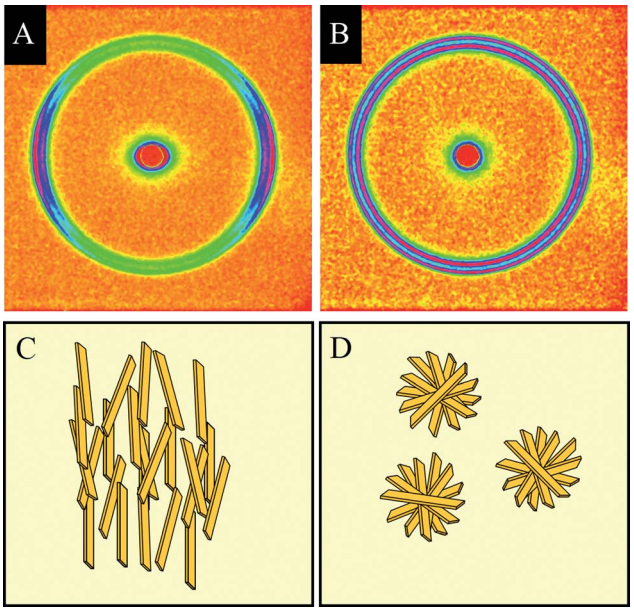

Fig. 8 Synchrotron small-angle X-ray diffraction patterns for a mixture of 70% trilaurin and 30% trimyristin (7L3M) dissolved in triolein (OOO) in a 3 : 2 proportion of OOO: 7L3M crystallized at 14 °C under a shear rate of 80 s^{-1} (A) and a shear rate of 0 s^{-1} (B). The X-ray scattering anisotropy observed in (A) is due to the orientation of the fat crystal nanoplatelets parallel to the direction of the shear field (C). The isotropic scattering observed in (B) is due to the random arrangement of the fat crystal nanoplatelets (D).

and the applied shear rate. This included the formation of a fractionated phase dubbed "phase X".[151] At moderate shear rates and low crystallization temperatures (17.5 °C), cocoa butter crystallized initially in form II, and then transformed into a mixture of form V and phase X. The amount of form II left after the phase transition decreased with increasing shear rates. Increasing the shear rate also decreased the amount of phase X formed. At higher shear rates, the short-lived phase II disappeared completely, and phase V was formed without the concomitant formation of phase X. Phase X was later obtained under static conditions using slow cooling rates,[150] reinforcing the notion that this phase forms during fractionation. The following results show that the polymorphic forms obtained during fat crystallization can be engineered using shear-temperature combinations.

X-Ray diffraction and microscopy studies of fat crystallized under oscillatory shear flow by Sonwai and Mackley showed that the onset of phase V under shear flow was not due to an initial change or melting of the existing phase II. Rather, phase V nucleated on the existing phase II solids, followed by the melting and re-crystallization of the pre-existing phase II.[161] This was consistent with other findings.[150,162]

The effect of shear on the polymorphic form was made even more clear when mechanical and thermal data on cocoa butter crystallized in a special Couette shear cell were obtained.[163,164] It was apparent that different combinations of shear and temperature produced different mechanical and thermal properties. Furthermore, there appeared to be a critical shear rate, around 360 s^{-1}, which delineated whether or not the effects occurred. Above this critical shear rate, the material was generally stronger (higher peak breaking force) and had higher melting points than fat materials crystallized below the critical shear rate. The difference in the melting point was attributed to the crystallization of the lower-melting TAGs into the β_{VI} polymorph. It was also shown that the orientation effect was observed only at shear rates above the critical shear rate.[164]

A recent study by Maleky and Marangoni[48] showed that the application of shear during cocoa butter crystallization resulted in a material with a higher breaking force, Young's modulus and elastic storage modulus (G'). The crystals developed under shearing conditions were also much smaller than the crystals developed under static conditions. However, contrary to the results observed by Guthrie,[164] a slight decrease in the melting point (by about 0.5 °C) was observed.

A recent rheo-NMR study on the crystallization of cocoa butter[162] showed that the solid fraction in sheared cocoa butter did not rise above 50% at crystallization temperatures between 17.5 and 22.5 °C and shear rates between 45 and 720 s^{-1}. As well, the synchrotron X-ray diffraction data indicated a different phase composition for the cocoa butter crystallized at shear rates of 360 s^{-1} and above. It is clear that there is no simple way to summarize the effect that cooling rate, final temperature, shear rate and time have on the final characteristics of cocoa butter. Some general ideas can be outlined as follows: slow cooling rates and high crystallization temperatures tend to favour the formation of the "intermediate" form β'_{IV}, followed by a transformation into the form β_V. On the other hand, low crystallization temperatures and high shear rates tend to produce a rapid transition from α_{II} to β_V or β_{VI}. The resulting material has a somewhat lower melting point but possesses a more stable structure and is much harder. A systematic research on chocolate products is still necessary to establish how these general trends apply. The non-fat particles in the chocolate modify the effective local shear rate of the cocoa butter, and generate more viscous heat. An equivalence of conditions should be estimated, and nanostructural studies carried at those conditions. There have been some studies on chocolate itself[157–160] but they focused mostly in macroscopic properties or on the visible microstructure as affected by the tempering conditions.

Studies in other fat systems also indicate that shear can accelerate the transformation of polymorphs to a more stable phase, so long as the viscous heat generated by shearing is not excessive. These studies also suggest the orientation of fat crystals. These studies have been conducted in-situ using X-ray diffraction,[33,152–155,165] rheology,[166–171] microscopy and NMR.[115,172,173] The thermal and mechanical properties of the materials have also been studied. Two interesting observations from these studies are that the *d*-spacing decreases as transformation to the more stable phase proceeds, and that the range of thicknesses of the nanoplatelets is more or less within 20–150 nm, though these can be modified by changes in the temperature of crystallization.

An interesting observation is that the differential form of the Avrami model (JMAEK model) works very well to describe growth under shear flow. This is because the particles are better separated and surrounded by liquid, and the liquid is more homogeneous due to the mixing induced by the shear.[152,153]

 This journal is © The Royal Society of Chemistry 2012

View Article Online

Published on 11 November 2011. Downloaded by Michigan State University on 19/01/2016 06:25:56.

The viscosity of the suspension is strongly affected by the shear rate. The crystallizing suspension shows pseudoplastic behavior with the viscosity decreasing as the shear rate is increased. A typical temperature ramp curve of the crystallizing suspension shows several sections:[167] a gradual increase in viscosity while the melt is being cooled down, a sudden exponential increase attributable to crystals formed during the first crystallization event, and a second, much larger 'jump' due to a phase transition to a more stable form. As the crystallization progresses, the viscosity reaches a maximum and then decreases (Fig. 9). The decrease can be abrupt or gradual, but is almost always present. This can be explained by the formation of a dynamic structure in the liquid suspension. As the solid fraction increases, the viscosity increases. At some point, the interaction between clusters of nanoplatelets is such that there is a breakdown into smaller clusters and free platelets, progressively transforming to a dynamic steady state. This steady state can take a long time to reach. In some instances, after 2 hours of shear-crystallization, the viscosity is still decreasing. The initial gradual increase in viscosity correlate well with XRD and NMR data, since an increase in viscosity is observed in conjunction with an increase in the intensity of an X-ray peak or an increase in the solids fraction content. In the latter stages, it is clear that it is not a decrease in the total crystalline mass that is causing the viscosity decrease, but rather a structural re-organization.

From these fundamental concepts, a patent for a practical application has been developed,[174] and a laminar shear crystallizer has been used to study the crystallization process under shear flow.[48,175] Some of the findings from these studies have been already discussed.

To develop a comprehensive understanding of the effect of shear flow fields on the crystallization of fats, it is essential that a nanoscale "bottom-up" perspective be adopted. Thus, the observed processes can be understood from a common foundation. The formation of nanoplatelets begins with nucleation events, in which the platelet components must overcome the free energy barrier associated with the formation of a surface and the decrease in entropy associated with their ordering.[33] At a given shear rate, depending on the temperature and the temperature history of the material,[176] there will be a number of competing processes taking place in the liquid. The crystallization temperature may be below the melting point of several potential crystallizing species (different polymorphism and composition) and thus the divergent formation/disruption of embryos around nucleation sites may result in more than one phase. If the embryos reach length scales sensitive to shear forces,[33,155] then an effect during the first onset of crystallization will be observed. However, this is not apparent in studies reviewed above, perhaps because the undercoolings involved are too large. What is clear, however, is a strong effect on subsequent nucleation events.[150,161] It is thus reasonable to think that the application of shear reduces the free energy for the formation of the more stable phases. The mechanism by which this occurs, however, is vague. It is possible that this effect is due to the fact that shear affects the spatial distribution of the nanocrystals or that it mixes liquid surrounding the solid nuclei, thus enhancing heat and mass transfer. This subsequently reduces the Gibbs free energy barrier for the formation of more stable phases.

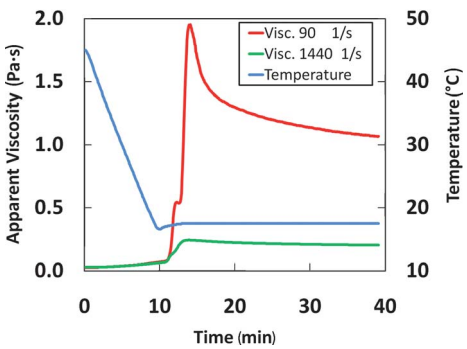

Fig. 9 The evolution of the viscosity of anhydrous milk fat (AMF) crystallized from the melt at 45 °C to 17.5 °C at a cooling rate of 3 °C min^{-1}. AMF was crystallized under two different shear rates, 90 and 1440 s^{-1}. The viscosity at the shear rate of 1440 s^{-1} is much lower. After attaining a peak viscosity, the viscosity of shear-crystallized AMF decreased under both shear rates, ostensibly due to disintegration of nanocrystal aggregates.

Crystallization under static conditions causes the nanocrystals to aggregate, forming large aggregates with a small surface to volume ratio. The application of shear, on the other hand, reduces the aggregation of the platelets as well as promoting the "exchange" of platelets between "clusters" and free nanoplatelets. Where the platelet is un-aggregated, it can adopt and orientation relative to the flow field. In addition, the entire surface of a free nanoplatelet is exposed to the oil. This would not be the case in nanoplatelet aggregates, as part of the surface of a nanoplatelet would be in contact with other nanoplatelets. The enormous increase in surface area to volume ratio that this produces will have a very significant impact on the nucleation of more stable forms from the liquid phase. The high surface area can also facilitate the melting and recrystallization of unstable crystalline forms of high-melting species that crystallized at the beginning of crystallization the process.[150] It is clear from X-ray diffraction data that this is the mechanism by which shear exerts its effects on phase transformations.

Effects of field combinations

The interaction of momentum, heat and mass transfer during crystallization and its effects in industrial equipment need to be better defined. It is clear that the application of shear enhances heat and mass transfer. Thus, the heat generated by crystallization and by viscous heating is transported from the material to the wall of the heat exchanger. In most systems, only one wall of the heat exchanger is cooled. A gradient of temperature develops in the material, and therefore gradients in viscosity and thermal generation are obtained. Coupled with the differences in local crystallization, there will be gradients in the composition of the liquid. This is particularly important in systems with a high relative curvature, *i.e.* wide gaps. However the non-Newtonian nature of the nanocrystalline and microcrystalline suspensions make this a particularly challenging subject yet to be explored for these materials.

A case study: effect of shear fields on transport properties of a fat network

As we have seen, a very large number of products depend for their mechanical and thermal properties on the space distribution

View Article Online

Published on 11 November 2011. Downloaded by Michigan State University on 19/01/2016 06:25:56.

and link strength of a fat crystal network. However, the space occupied by the entrapped liquid oil is no less important. The ability of a network to keep this oil is essential for its stability. The viscoelastic behavior of the material depends on the distribution of the liquid, and its diffusion properties depend on the liquid's ability to move in the network. We have included this case study to illustrate the strong effect that a shear field can have on the formation of the network structure, and its subsequent impact on the oil transport characteristics of the material. Recent work by Maleky and Marangoni[177] characterized the effect of laminar shear on the migration kinetics of oil through a cocoa butter matrix. The study employed static (no shear crystallization) conditions and two types of shear: a "mixing" shear where the cocoa butter was agitated during crystallization but no orientation was induced and an "orienting" shear (in the order of 340 s^{-1}) in which the cocoa butter fat crystals were oriented.

After 7 days "maturing" at 20 °C all specimens were in the β (triclinic) polymorphic form and had reached a solid fat content of approximately 78%, regardless of applied shear.

A sheet of crystallized cocoa butter was placed adjoining a "cream filling" material composed of peanut oil and interesterified hydrogenated palm oil stained with Nile red dye. The cream filling was positioned in three different arrangements relative to the shear plane. The rate of oil migration was quantified by tracking the movement of the dye through the cocoa butter matrix using a flatbed scanner. A rapid movement of the dye front was observed in the static samples and a lower migration rate in the shear-crystallized samples. An apparent coefficient of diffusion of the dye in the cocoa butter matrices was calculated using an approximate diffusion-based equation provided by Ziegleder[144,178] and used by others:[179–183]

$$D_{\text{eff}} = \left(\frac{m_t}{m_s}\frac{V}{KA}\frac{1}{\sqrt{t}}\right)^2 \tag{30}$$

where m_t and m_s are the migrated mass at time t and at saturation; A is the contact area between the two phases (m^2), V is the volume through which the diffusion takes place (m^3), and t is the migration time (s). D_{eff} is a time-dependent analogue of the diffusion coefficient ($m^2\ s^{-1}$), and K is a constant specific to the two phases.[184] Table 1 shows the diffusion coefficients decreasing as applied shear went from nothing through mixing to orienting.

Liquid diffusion depends on solid fat content and the shape, size and number distribution of the solid mass. In this case all samples had a similar SFC of 78% and β_V polymorphic form. Using cryo-TEM, it was observed that static crystallization of cocoa butter displayed a more heterogeneous microstructure than that obtained under shear (Fig. 10). Additionally, the length and width of the nano-platelets were reduced from 2000 nm × 165 nm in statically crystallized to 300 nm × 130 nm in sheared samples. Similar trends in thickness as affected by shear were observed previously by Mazzanti *et al.*[150] The larger fundamental particles explain the higher rate of diffusion in the statically crystallized materials.

The preferential alignment of the platelet surfaces parallel to the shear planes of the external shear field was the main structural difference between samples crystallized under mixing and under orienting conditions. The orientation reduced 3.8 times the apparent diffusivity, relative to static conditions. A lower oil migration rate was observed when the liquid was traveling parallel to the orientation. An even larger reduction was achieved when the oil was migrating normal to the orientation planes.

The porosity and the pores' connectivity are characterized by a tortuosity ratio, τ, that relates the diffusion coefficient in a bulk fluid to the effective diffusion coefficient over a long period of time:[185–188]

$$\tau = \frac{D_0}{D_{\text{eff}}} \tag{31}$$

where D_0 is the bulk fluid diffusion coefficient. Tortuosity is a function of the number of solid fat crystals, the distribution of the particles and the platelet aspect ratio.[189,190]

The tortuosity factors are present in Table 1. The tortuosity in the shear-crystallized samples was approximately 4 times higher than that of the static sample. This can be explained by the decrease in the average particle size from 2085 nm (in the static sample) to 385 nm (in the sheared sample), which provides a longer path for oil migration. The increase in tortuosity with aligned layers of crystals is illustrated in Fig. 11. A similar trend was observed when the network's porosity (the ratio of volume of pores to the total volume) was also considered in the calculation of the tortuosity factor:

$$\tau = \varepsilon\frac{D_0}{D_{\text{eff}}} \tag{32}$$

Two different definitions of porosity were used and the calculated tortuosity factors are presented in Table 1. In theory, porosity is the volume fraction of the void space, which in a fat network, is the nonsolid portion. Most of the studies that discuss tortuosity[190,191] consider the void fraction as $\varepsilon = 1 - \text{SFC}/100$, thus $\varepsilon = 0.22$ for all samples.

Table 1 Effective diffusivity of Nile red dissolved in liquid oil (D_{eff}) through a cocoa butter polycrystalline matrix, and the corresponding network permeability coefficients and tortuosity factors (τ)[a]

		Tortuosity			
Sample	$D_{\text{eff}}/m^2\ s^{-1}$	$\tau = D_0/D_{\text{eff}}$	$\tau = (1-\phi)(D_0/D_{\text{eff}})$	$\tau = \varepsilon\ (D_0/D_{\text{eff}})$	Permeability coefficient/m^2
Static	[b]7.57×10^{-12}	1.09	0.24	0.30	8.36×10^{-12}
Sheared	[c]3.03×10^{-12}	2.67	0.59	0.34	2.85×10^{-13}
Oriented	[d]1.97×10^{-12}	3.99	0.88	0.53	2.73×10^{-14}

[a] ε = volume fraction of network pores determined by polarized light microscopy and image analysis. ϕ = mass fraction of solids determined by pulsed NMR. Values with different superscript letters (b,c,d) are significantly different ($P < 0.05$).

 This journal is © The Royal Society of Chemistry 2012

View Article Online

Published on 11 November 2011. Downloaded by Michigan State University on 19/01/2016 06:25:56.

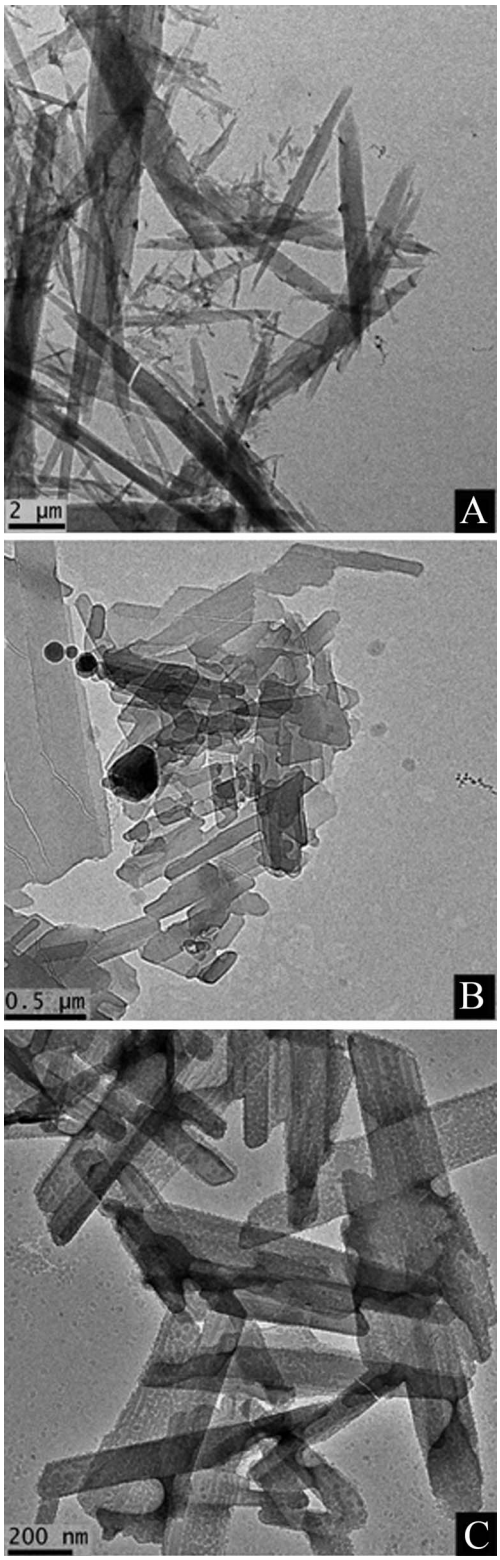

Fig. 10 Cryo-TEM micrographs of cocoa butter nanoplatelets crystallized under various shearing conditions. (A) 0 s^{-1}, (B) shear-mixed (340 s^{-1}) and (C) shear-oriented (340 s^{-1}).

An alternate method to estimate the tortuosity was to calculate the volume fraction of the pores (porosity) from polarized light micrographs of the crystallized samples. Although the calculated tortuosity factors obtained by different methods, shown in

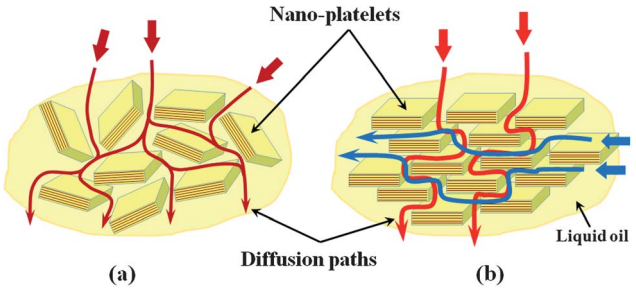

Fig. 11 A schematic illustration of the tortuosity of the diffusive path in cocoa butter crystallized under various shearing conditions. (A) Shear-mixed cocoa butter crystals showing a random arrangement of crystals. (B) Oriented cocoa butter crystals formed under laminar shear in a Couette-type device.

Table 1, present similar trends, they are certainly different. Their value below 1 indicates the presence of convective flow in the samples. Thus Darcy's law permeability coefficient B was calculated for each structure by means of eqn (33):

$$B = \frac{a^2}{\tau}\phi^{2/(D-3)} \tag{33}$$

where a is the particle diameter, ϕ is the solid volume fraction and D is the box-counting fractal dimension of the crystal network determined from polarized light microscopy images.[65,192] The 2d fractal dimension was converted to a 3d fractal dimension by $D_{3d} = D_{2d} + 1$. The cocoa butter network's permeability was reduced by about a factor of 100 by performing the crystallization process under laminar shear, due to the network changes in particle size, shape, orientation and spatial distribution, for the same solid content.

7. Outlook

In this review, we have examined the various structural features of fats from the crystallographic level all the way to the mesoscopic level, the size range just beyond which our eyes can resolve. We have shown that a rich structural hierarchy exists within triglyceride systems, with each level's properties and behavior directly dependent on the level below it. The formation of crystalline nanoplatelets is affected by the crystallization behavior of triglyceride molecules. In turn, the polycrystalline aggregates are influenced not only by the properties of the nanoplatelets but also by their mode of assembly. The characteristics of these polycrystalline aggregates then influence the properties and formation of the resulting fat crystal network. Ultimately, this fat crystal network is responsible for the functional properties of the fat as we perceive it. We have also shown that the properties of these structural levels at different length scales can be engineered by modifying certain physical parameters in the form of external fields such as temperature and flow.

In this outlook section, I would like to offer some of the lead author's *opinions* of what some of research priorities in this field might be. This is not supposed to be an exhaustive list, or even a list of the most important areas, but a list of "major holes" in our understanding of fat structure and functionality. The most obvious area in need of detailed work is that of polymorphism. Fat polymorphism is characterized using the subcell concept—

View Article Online

Published on 11 November 2011. Downloaded by Michigan State University on 19/01/2016 06:25:56.

a subcell, within the unit cell, which arises due to the packing of the polyethylene chains of fatty acids, is used to characterize polymorphism. This approach implies that triglycerides are just a collection of alkanes, which they are not. Moreover, this approach breaks down when different types of polymorphs are present, forms V and VI in cocoa butter, for example. The subcell concept does not explain the structural difference between the two. With modern computational power accessible to anyone using powder X-ray diffraction, why not use the true unit cell of a triglyceride crystal to classify polymorphs? This is not a trivial pursuit since we are dealing with multicomponent systems with complex phase behavior. The recent efforts by Peschar *et al.*[25] are of particular value. Even though they managed to propose the solid state structure of cocoa butter crystals based on the known structure of the major triglyceride present (SOS), they were not able to index even high-resolution synchrotron powder patterns using modern techniques. This suggests that indexing patterns for these complex multicomponent systems is not trivial. However, I do believe it is not impossible either. Secondly, the recent discovery by our group[34,35,44] of the existence of a well defined nanoscale structure underlying all structure in fats should be studied much more thoroughly. New ways of quantifying this level of structure without having to resort to lengthy extraction techniques need to be developed. We need a nanoplatelet "sizer". This would allow researchers to quantify the properties of the true primary crystal present in the network. The idea that fat crystals are micron sized objects should be abandoned. Even though the topic of crystal aggregation is of major interest to the authors of this paper, we need to better understand how nanoplatelets aggregate into larger mesoscale structures, if anything to learn how to prevent it from happening—at least in applications such as butter, margarine and shortening manufacture. Last, but not least, is the development of an understanding of the factor responsible for the properties of laminating fats or "roll-in" shortenings. These materials are truly amazing. A roll-in shortening used in the manufacture of croissants, and other such "laminates", is a true challenge. Imagine a material that can be extruded into micron width films and must withstand pressures of up to 50 kPa.[193] It is simple to make a hard material, what is difficult is to make a fat hard and malleable. The fat content of such products is 30% by weight, or more. The reduction of the "hard fat" content (saturated and *trans*) in these products is a world-wide priority for many multinationals. The first group that reaches the finish line will reap enormous benefits and make an important contribution towards the health of many communities.

Fisher–Turnbull equation

τ	induction time of nucleation, s
T	temperature, K
α	Boltzmann partition function related to the free energy of activation for diffusion, *non-dimensional and* $0 \leq \alpha < 1$.
γ	interfacial tension, N m^{-1}
V_{m}s	molar volume, m^3 mol^{-1}
T_m	melting point, K
ΔH_m	melting enthalpy, J mol^{-1}
ΔT	undercooling, K
$\Delta G_n r$	free energy of nucleation, J per nucleus

Avrami equation

SFC	solid fat content, *non-dimensional*
SFC_{max}	solid fat content at equilibrium, *non-dimensional*
k_A	Avrami growth constant, t^{-n}
t	time, s
n	Avrami index, *non-dimensional*

Models of crystalline nanoplatelets (CNPs)

$V(r)$, $V_A(r)$	interaction energies, J
V_0	binding energy, J
R	sphere radius, m
r	centre-to-centre sphere distance, m
s	shortest distance between surfaces of spheres possessing centre-to-centre distance of r, m
δ	a small distance defining the range of the binding energy V_0, m
A, A_H	Hamaker coefficient, J
k_B	Boltzmann's constant, J K^{-1}
T	absolute temperature, K
m, L	positive integers defining the size of the crystalline nanoplatelets and the simulation volume, respectively

Monte Carlo computer simulation. Metropolis algorithm

E_i, E_f	energies of the initial and final states in an attempt to change the state of a system in a Monte Carlo simulation. $\Delta E = E_f - E_i$
y	random number with $0 \leq y < 1$, $\beta = 1/k_B T$, J^{-1}

Static structure function

$S_f(\vec{q})$	the Fourier transform of a pair correlation function; a quantity that yields information about the structure of a system
$I(\vec{q})$	the intensity measured by X-ray or neutron scattering; in this case, $S_f(\vec{q}) = I(\vec{q})$
$\vec{q}$	wavevector conjugate to general position vector, $\vec{r}$, and appearing in the Fourier transform as exp ($i\vec{q}\vec{r}$)
$S_f(q) = \langle S_f(\vec{q})\rangle_{\lvert\vec{q}\rvert=q}$	the structure function averaged over all $\vec{q}$ vectors of the same magnitude

This journal is © The Royal Society of Chemistry 2012

View Article Online

Published on 11 November 2011. Downloaded by Michigan State University on 19/01/2016 06:25:56.

$\ell = 2\pi/q$	the characteristic length that results in scattering of radiation of wavevector magnitude q, nm
D	the fractal dimension detected by scattering; in that case, $S_f(q) \approx q^{-D}$

Dispersion forces

d	distance between two fats particles, m
$\varepsilon_{ra}(\omega)$	the relative frequency-dependent electrical permittivity for a medium labelled a, F m^{-1}
$i\xi_m$	the Matsubara frequencies. Summing over these frequencies is a useful technique taken from quantum field theory and adapted to quantum statistical mechanics
n_k	the refractive index of a medium labeled k
ν_{UV}	the electronic frequency in the ultraviolet region of the electromagnetic spectrum, s^{-1}
h	Planck's constant, J s

The fractal model

G'	the storage modulus, Pa
ϕ	the solid fraction of fats in a floc, *non-dimensional*
a	the diameter of a fat floc component, m
λ	the slope of ln G' with respect to ln ϕ, Pa
γ	is the strain at the limit of linearity, *non-dimensional*
d_0	the equilibrium distance between the floc components, m

The semi-classical model

μ	the disjoining interfacial free energy per unit area of two blocks of fats formed from a single block
d_e	The equilibrium separation of the two blocks of fats formed from the disjoining

Lenard-Jones potential

$u_{AB}(r) = -\frac{C_6^{AB}}{r^6} + \frac{C_{12}^{AB}}{r^{12}}$	the interaction energy of a pair of atoms, A and B, with a centre-to-centre separation, r
$\Phi_i(\vec{r})$	the number density (number of objects per unit volume) of objects of type i at spatial position, $\vec{r}$
U_{123}	the energy of interaction of two objects (fats), 1 and 2, separated by a medium (oil) 3

Atomic scale molecular dynamics. Thermodynamics

NpT ensemble	the system is defined by a fixed number of molecules at constant pressure and temperature
NVT ensemble	the system is defined by a fixed number of molecules at constant volume and temperature

Structural-mechanical models

G	shear modulus, Pa
A	Hamaker's constant, J
Φ	solids volume fraction, *non-dimensional*
a	primary particle diameter, m
H_0	interparticle distance, m
n	number of connecting chains between two neighboring aggregates
N	average number of primary particles in an aggregate
D_a	average diameter of an aggregate, m
E	Young's modulus, Pa
ΔU_ξ	change in the internal energy per floc–floc bond, J
l_0	effective distance between flocs, m
l	distance between flocs under an applied stress, m
ξ	diameter of the flocs, m
ε	compressive strain of the network ($\varepsilon = \Delta L/L$, where ΔL is the deformation of the network and L is the size of the network), *non-dimensional*
d	Euclidean dimension of the embedding space, *non-dimensional*
D	fractal dimension for the arrangement, *non-dimensional*

Effects of external fields on structure and oil binding capacity

A	crosssectional area of the material in which the diffusion is happening, m^2
a	particle diameter, m
B	Darcy's law permeability coefficient, m^2
d	characteristic long spacing between two planes producing the X-ray diffraction peak from the nanocrystalline platelets of a given solid phase, in nm
D	fractal dimension of the solid network, non-dimensional

View Article Online

Published on 11 November 2011. Downloaded by Michigan State University on 19/01/2016 06:25:56.

D_0	molecular diffusivity in the absence of the solid matrix, $m^2\ s^{-1}$
D_{eff}	effective or apparent diffusivity in the presence of the solid matrix, $m^2\ s^{-1}$
ε	porosity, either ratio of volume filled with oil to total volume, or ratio of volume effectively available for diffusion to total volume, non-dimensional
K	characteristic constant for the two phases in contact, non-dimensional
m_s	mass of material diffused into the matrix at saturation, kg
m_t	mass of material diffused into the matrix at time t, kg
t	time, s
V	total volume of the material in which the diffusion is happening, m^3
Δq	full width at half maximum of the small angle X-ray diffraction peak produced by a given solid phase, in coordinates of the scattering vector $\boldsymbol{q}$ defined as $\boldsymbol{q} = 2\pi/d$, nm^{-1}
ξ	average thickness (determined by X-ray diffraction) of the nanocrystalline platelets of a given solid phase, nm
τ	tortuosity of the network, *non-dimensional*
ϕ	volume fraction of solids in the material, *non-dimensional*

References

1 B. D. Dixon and J. V. Parekh, *J. Texture Stud.*, 1979, **10**, 421–434.
2 M. Hayakawa and J. M. deMan, *J. Texture Stud.*, 1982, **13**, 201–210.
3 D. Rousseau and A. G. Marangoni, *Food Res. Int.*, 1999, **31**, 381–388.
4 J. M. deMan and A. M. Beers, *J. Texture Stud.*, 1987, **18**, 303–318.
5 K. M. Flegal, M. D. Carroll, C. L. Ogden and L. R. Curtin, *JAMA, J. Am. Med. Assoc.*, 2010, **303**, 235–241.
6 R. P. Mensink and M. B. Katan, *N. Engl. J. Med.*, 1990, **323**, 439–445.
7 R. P. Mensink, P. L. Zock, A. D. M. Kester and M. B. Katan, *Am. J. Clin. Nutr.*, 2003, **77**, 1146–1155.
8 D. Mozaffarian, M. B. Katan, A. Ascherio, M. J. Stampfer and W. C. Willett, *N. Engl. J. Med.*, 2006, **354**, 1601–1613.
9 A. Ascherio, M. B. Katan, P. L. Zock, M. J. Stampfer and W. C. Willett, *N. Engl. J. Med.*, 1999, **340**, 1994–1998.
10 A. Keys, *JAMA, J. Am. Med. Assoc.*, 1957, **164**, 1912–1919.
11 *Harvard School of Public Health Website*, http://www.hsph.harvard.edu/nutritionsource/what-should-you-eat/fats-full-story/index.html.
12 A. G. Marangoni, in *Fat Crystal Networks*, ed. A. G. Marangoni, Marcel Dekker, New York, 1st edn, 2005, ch. 2, pp. 21–82.
13 J. W. Gibbs, *The Collected Works of J. Willard Gibbs Volume 1—Thermodynamics*, Longmans Green and Co., New York, 1928.
14 D. Turnbull and J. C. Fisher, *J. Chem. Phys.*, 1949, **17**, 71–73.
15 R. Campos, M. Ollivon and A. G. Marangoni, *Cryst. Growth Des.*, 2010, **10**, 205–217.
16 L. Ahmadi, A. J. Wright and A. G. Marangoni, *Food Biophys.*, 2009, **4**, 64–76.
17 A. G. Marangoni and S. E. McGauley, *Cryst. Growth Des.*, 2003, **3**, 95–108.
18 S. S. Narine and A. G. Marangoni, *Phys. Rev. E: Stat. Phys., Plasmas, Fluids, Relat. Interdiscip. Top.*, 1999, **60**, 6991–7000.
19 S. S. Narine and A. G. Marangoni, *Food Res. Int.*, 1999, **32**, 227–248.
20 A. G. Marangoni, *Phys. Rev. B: Condens. Matter*, 2000, **62**, 13951–13955.
21 A. G. Marangoni and M. A. Rogers, *Appl. Phys. Lett.*, 2003, **82**, 3239–3241.
22 L. H. Jensen and A. J. Mabis, *Nature*, 1963, **197**, 681–682.
23 L. H. Jensen and A. J. Mabis, *Acta Crystallogr.*, 1966, **21**, 770–781.
24 A. van Langevelde, R. Peschar and H. Shenk, *Acta Crystallogr., Sect. B: Struct. Sci.*, 2001, **57**, 372–377.
25 R. Peschar, M. P. Mihaela, D. J. A. de Ridder, J. B. van Mechelen, R. A. J. Driessen and H. Schenk, *J. Phys. Chem. B*, 2004, **108**, 15450–15453.
26 M. Goto, D. R. Kodali, D. M. Small, K. Honda, K. Kozawa and T. Uchida, *Proc. Natl. Acad. Sci. U. S. A.*, 1992, **89**, 8083–8086.
27 K. Sato, M. Goto, J. Yano, K. Honda, D. R. Kodali and D. M. Small, *J. Lipid Res.*, 2001, **42**, 338–345.
28 A. van Langevelde, K. van Malssen, R. Driessen, K. Goubitz, F. Hollander, R. Peschar, P. Zwart and H. Schenk, *Acta Crystallogr., Sect. B: Struct. Sci.*, 2000, **56**, 1103–1111.
29 S. M. Hodge and D. Rousseau, *J. Am. Oil Chem. Soc.*, 2002, **79**, 1115–1121.
30 D. M. Small, *The Physical Chemistry of Lipids*, Plenum Press, New York, 1986.
31 K. Sato, *Chem. Eng. Sci.*, 2001, **56**, 2255–2265.
32 G. Mazzanti, S. E. Guthrie, E. B. Sirota, A. G. Marangoni and S. H. J. Idziak, *Cryst. Growth Des.*, 2004, **4**, 1303–1309.
33 G. Mazzanti, S. E. Guthrie, E. B. Sirota, A. G. Marangoni and S. H. J. Idziak, *Cryst. Growth Des.*, 2003, **3**, 721–725.
34 N. C. Acevedo and A. G. Marangoni, *Cryst. Growth Des.*, 2010, **10**, 3334–3339.
35 N. C. Acevedo and A. G. Marangoni, *Cryst. Growth Des.*, 2010, **10**, 3327–3333.
36 G. G. Jewell and M. L. Meara, *J. Am. Oil Chem. Soc.*, 1970, **47**, 535–538.
37 C. Poot, W. Dijkshoorn, A. J. Haighton and C. C. Verburg, *J. Am. Oil Chem. Soc.*, 1975, **52**, 69–72.
38 I. Heertje, M. Leunis, W. J. M. van Zeyl and E. Berends, *Food Microstruct.*, 1987, **6**, 1–8.
39 P. Chawla and J. M. deMan, *J. Am. Oil Chem. Soc.*, 1990, **67**, 329–332.
40 T. Unruh, K. Westesen, P. Bösecke, P. Lindner and M. H. J. Koch, *Langmuir*, 2002, **18**, 1796–1800.
41 H. Bunjes, F. Steiniger and W. Richter, *Langmuir*, 2007, **23**, 4005–4011.
42 I. Heertje and M. Leunis, *Lebensm.-Wiss. Technol. (1968–2004)*, 1997, **30**, 141–146.
43 A. R. West, *Solid State Chemistry and its Applications*, John Wiley & Sons, Chichester, England, 1984.
44 N. C. Acevedo, F. Peyronel and A. G. Marangoni, *Curr. Opin. Colloid Interface Sci.*, 2011, **16**, 374–383.
45 A. G. F. Stapley, H. Tewkesbury and P. J. Fryer, *J. Am. Oil Chem. Soc.*, 1999, **76**, 677–685.
46 A. Rodriguez, E. Castro, M. C. Salinas, R. Lopez and M. Miranda, *J. Am. Oil Chem. Soc.*, 2001, **78**, 431–436.
47 A. P. B. Ribeiro, R. Grimaldi, L. A. Gioielli, A. Oliveira dos Santos, L. P. Cardoso and L. A. G. Goncalves, *Food Biophys.*, 2009, **4**, 106–118.
48 F. Maleky and A. G. Marangoni, *Cryst. Growth Des.*, 2011, **11**, 2429–2437.
49 F. Maleky, A. K. Smith and A. G. Marangoni, *Cryst. Growth Des.*, 2011, **11**, 2335–2345.
50 A. L. Fogelson, *J. Comput. Phys.*, 1984, **56**, 111–134.
51 A. L. Fogelson, *SIAM J. Appl. Math.*, 1992, **52**, 1089–1110.
52 V. A. Parsegian, *van der Waals Forces: a Handbook for Biologists, Chemists, Engineers, and Physicists*, Cambridge University Press, New York, 2005.
53 J. N. Israelachvili, *Intermolecular and Surface Forces*, Academic Press, London, 2006.
54 *GROMACS Website*, http://www.gromacs.org/Documentation/Manual.
55 K. Binder and D. Heermann, *Monte Carlo Simulation in Statistical Physics: an Introduction*, Springer-Verlag, Berlin, 5th edn, 2010.
56 I. Carmesin and K. Kremer, *Macromolecules*, 1988, **21**, 2819–2823.
57 D. P. Landau and K. Binder, *A Guide to Monte Carlo Simulations in Statistical Physics*, Cambridge University Press, New York, 2nd edn, 2005.
58 M. van den Tempel, *J. Colloid Sci.*, 1961, **16**, 284–296.
59 C. J. Nederveen, *J. Colloid Sci.*, 1963, **18**, 276–291.

 This journal is © The Royal Society of Chemistry 2012

View Article Online

Published on 11 November 2011. Downloaded by Michigan State University on 19/01/2016 06:25:56.

60 M. van den Tempel, *J. Colloid Interface Sci.*, 1979, **71**, 18–20.
61 D. Tang and A. G. Marangoni, *J. Am. Oil Chem. Soc.*, 2008, **85**, 495–499.
62 R. H. French, V. A. Parsegian, R. Podgornik, R. F. Rajter, A. Jagota, J. Luo, D. Asthagiri, M. K. Chaudhury, Y. Chiang, S. Granick, S. Kalinin, M. Kardar, R. Kjellander, D. C. Langreth, J. Lewis, S. Lustig, D. Wesolowski, J. S. Wettlaufer, W. Y. Ching, M. Finnis, F. Houlihan, O. A. von Lilienfeld, C. J. van Oss and T. Zemb, *Rev. Mod. Phys.*, 2010, **82**, 1887–1944.
63 I. E. Dzyaloshinskii, E. M. Lifshitz and L. P. Pitaevskii, *Sov. Phys. Usp.*, 1961, **4**, 153–176.
64 H. C. Hamaker, *Physica*, 1937, **4**, 1058–1072.
65 L. Ahmadi, A. J. Wright and A. G. Marangoni, *Eur. J. Lipid Sci. Technol.*, 2008, **110**, 1014–1024.
66 P. C. Hiemenz and R. Rajagoplalan, *Principles of Colloid and Surface Chemistry*, Marcel Dekker, New York, 3rd edn, 1997.
67 Z. Y. Yan, S. D. Huhn, L. P. Klemann and M. S. Otterburn, *J. Agric. Food Chem.*, 1994, **42**, 447–452.
68 A. K. Sum, M. J. Biddy and J. J. dePablo, *J. Phys. Chem. B*, 2003, **107**, 14443–14451.
69 A. Hall, J. Repakova and I. Vattulainen, *J. Phys. Chem. B*, 2008, **112**, 13772–13782.
70 W. D. Hsu and A. Violi, *J. Phys. Chem. B*, 2009, **113**, 887–893.
71 H. J. C. Berendsen, D. van der Spoel and R. Vandrunen, *Comput. Phys. Commun.*, 1995, **91**, 43–53.
72 C. Kutzner, D. van der Spoel, M. Fechner, E. Lindahl, U. W. Schmitt, B. L. de Groot and H. J. Grubmuller, *J. Comput. Chem.*, 2007, **28**, 2075–2084.
73 J. Berger, O. Edholm and F. Jähnig, *Biophys. J.*, 1997, **72**, 2002–2013.
74 D. Johansson and B. Bergenståhl, *J. Am. Oil Chem. Soc.*, 1992, **69**, 718–727.
75 W. Kloek, PhD Thesis, Wageningen University and Research Centre, 1998.
76 J. Mittal, J. R. Errington and T. M. Truskett, *J. Chem. Phys.*, 2007, **126**, 244708–244716.
77 V. DeGrandis, P. Gallo and M. Rovere, *J. Mol. Liq.*, 2007, **134**, 90–93.
78 W. T. Huang and D. G. Levitt, *Biophys. J.*, 1977, **17**, 111–128.
79 I. Heertje, *Food Microstruct.*, 1993, **12**, 77–94.
80 A. C. Juriaanse and I. Heertje, *Food Microstruct.*, 1988, **7**, 181–188.
81 A. G. Marangoni and D. Rousseau, *J. Am. Oil Chem. Soc.*, 1996, **73**, 991–994.
82 S. S. Narine and A. G. Marangoni, *Lebensm.-Wiss. Technol. (1968–2004)*, 2001, **34**, 33–40.
83 B. Liang and R. W. Hartel, *J. Dairy Sci.*, 2004, **87**, 20–31.
84 A. J. Wright, M. G. Scanlon, R. W. Hartel and A. G. Marangoni, *J. Food Sci.*, 2008, **66**, 1056–1071.
85 A. G. Marangoni, *Trends Food Sci. Technol.*, 2002, **13**, 37–47.
86 P. Sherman, *Proceedings of the 5th International Conference on Rheology, Kyoto*, 1968.
87 A. R. Payne, *J. Colloid Sci.*, 1964, **19**, 744–754.
88 D. Rousseau and A. G. Marangoni, *J. Agric. Food Chem.*, 1998, **46**, 2375–2381.
89 D. Tang and A. G. Marangoni, *J. Am. Oil Chem. Soc.*, 2006, **83**, 377–388.
90 D. Tang and A. G. Marangoni, *Adv. Colloid Interface Sci.*, 2006, **128–130**, 257–265.
91 E. D. Dibildox-Alvarado, J. N. Rodrigues, L. A. Gioielli, J. F. T. Vazquez and A. G. Marangoni, *Cryst. Growth Des.*, 2004, **4**, 731–736.
92 D. Tang and A. G. Marangoni, *J. Am. Oil Chem. Soc.*, 2006, **83**, 309–314.
93 W. H. Shih, W. Y. Shih, S. I. Kim, J. Liu and I. A. Aksay, *Phys. Rev. A: At., Mol., Opt. Phys.*, 1990, **42**, 4772–4779.
94 R. Vreeker, L. L. Hoekstra, D. C. den Boer and W. G. M. Agterof, *Colloids Surf.*, 1992, **65**, 185–189.
95 T. S. Awad, M. A. Rogers and A. G. Marangoni, *J. Phys. Chem. B*, 2004, **108**, 171–179.
96 A. A. Griffith, *Philos. Trans. R. Soc. London, Ser. A*, 1921, **221**, 163–198.
97 T. Woignier and F. Despetis, *J. Sol-Gel Sci. Technol.*, 2000, **19**, 163–169.
98 P. D. Beale, *Phys. Rev. B*, 1988, **37**, 5500–5507.
99 S. G. Bardenhagen and J. U. Brackbill, *Phys. Rev. E: Stat. Phys., Plasmas, Fluids, Relat. Interdiscip. Top.*, 2000, **62**, 3882–3890.
100 W. Kloek, T. van Vliet and P. Walstra, *J. Texture Stud.*, 2005, **36**, 516–543.
101 L. Duffours, T. Woignier and J. Phalippou, *J. Non-Cryst. Solids*, 1995, **186**, 321–327.
102 H. Tanaka, *Phys. Rev. E: Stat. Phys., Plasmas, Fluids, Relat. Interdiscip. Top.*, 1999, **59**, 6842–6852.
103 R. Buscall, P. D. A. Mills, J. W. Goodwin and D. W. Lawson, *J. Chem. Soc., Faraday Trans. 1*, 1988, **84**, 4249–4260.
104 A. Emmerling and J. Fricke, *J. Sol-Gel Sci. Technol.*, 1997, **8**, 781–788.
105 C. J. Rueb and C. F. Zukoskia, *J. Rheol.*, 1997, **41**, 197–218.
106 A. P. Roberts and E. J. Garboczi, *J. Mech. Phys. Solids*, 2002, **50**, 33–55.
107 H. S. Ma, A. P. Roberts, J. H. Prevost, R. Jullien and G. W. Scherer, *J. Non-Cryst. Solids*, 2000, **277**, 127–141.
108 H. S. Ma, A. P. Roberts, J. H. Prevost, R. Jullien and G. W. Scherer, *J. Non-Cryst. Solids*, 2000, **277**, 127–141.
109 D. Tang and A. G. Marangoni, *J. Colloid Interface Sci.*, 2008, **318**, 202–209.
110 R. B. Bird, W. E. Stewart and E. N. Lightfoot, *Transport Phenomena*, John Wiley & Sons, Inc., New York, 2002.
111 R. G. Larson, *The Structure and Rheology of Complex Fluids*, Oxford University Press, Oxford, 1999.
112 J. H. Los and E. Floter, *Phys. Chem. Chem. Phys.*, 1999, **1**, 4251–4257.
113 J. H. Los and M. Matovic, *J. Phys. Chem. B*, 2005, **109**, 14632–14641.
114 M. Matovic, J. C. van Miltenburg, H. A. J. Oonk and J. H. Los, *CALPHAD: Comput. Coupling Phase Diagrams Thermochem.*, 2006, **30**, 209–215.
115 M. M. Britton, *J. Texture Stud.*, 2000, **31**, 245–255.
116 M. M. Britton, P. T. Callaghan, M. L. Kilfoil, R. W. Mair and K. M. Owens, *Appl. Magn. Reson.*, 1998, **15**, 287–301.
117 S. Ueno, R. I. Ristic, K. Higaki and K. Sato, *J. Phys. Chem. B*, 2003, **107**, 4927–4935.
118 S. Martini, A. Suzuki and R. Hartel, *J. Am. Oil Chem. Soc.*, 2008, **85**, 621–628.
119 A. Miura, A. Kusanagi, S. Kobayashi, S. Tokairin and Z. Jin, *IEEE Trans. Appl. Supercond.*, 2004, **14**, 1588–1591.
120 M. Miura, A. Kusanagi, S. Kobayashi, S. Tokairin and K. Tsurumi, *J. Oleo Sci.*, 2005, **54**, 193–202.
121 H. Lizhi, K. Toyoda and I. Ihara, *J. Food Eng.*, 2008, **88**, 151–158.
122 C. E. Kundrot, R. A. Judge, M. L. Pusey and E. H. Snell, *Cryst. Growth Des.*, 2000, **1**, 87–99.
123 D. Tang and A. G. Marangoni, *Chem. Phys. Lett.*, 2006, **433**, 248–252.
124 S. Martini, C. Bertoli, M. L. Herrera, I. Neeson and A. Marangoni, *J. Am. Oil Chem. Soc.*, 2005, **82**, 305–312.
125 R. Campos, in *Fat Crystal Networks*, ed. A. G. Marangoni, Marcel Dekker, New York, 1st edn, 2005, ch. 9, pp. 267–348.
126 A. Cisneros, G. Mazzanti, R. Campos and A. Marangoni, *J. Agric. Food Chem.*, 2006, **54**, 6030–6033.
127 M. Werner, A. Baars, C. Eder and A. Delgado, *J. Chem. Eng. Data*, 2008, **53**, 1444–1452.
128 R. Ramaswamy, V. M. Balasubramaniam and S. K. Sastry, *J. Food Eng.*, 2007, **83**, 444–451.
129 J. Coupland and D. McClements, *J. Am. Oil Chem. Soc.*, 1997, **74**, 1559–1564.
130 N. A. Morad, A. A. M. Kamal, F. Panau and T. W. Yew, *J. Am. Oil Chem. Soc.*, 2000, **77**, 1001–1005.
131 K. Van Putte, L. Vermaas, J. Van Den Enden and C. Den Hollander, *J. Am. Oil Chem. Soc.*, 1975, **52**, 179–181.
132 J. W. Hagemann and J. A. Rothfus, *J. Am. Oil Chem. Soc.*, 1983, **60**, 1123–1131.
133 A. A. Tarzimanov, R. A. Sharafutdinov and F. R. Gabitov, *J. Eng. Phys. Thermophys.*, 1990, **59**, 1334–1338.
134 V. A. Konstantinov, V. P. Revyakin and V. V. Sagan, *Fiz. Nizk. Temp.*, 2011, **37**, 531–534.
135 R. P. Singh and D. R. Heldman, *Introduction to Food Engineering*, Academic Press - Elsevier, San Francisco, 2009.
136 J. Crank, *The Mathematics of Diffusion*, Clarendon Press, Oxford, 1975.
137 E. Deffense, *Oléagineux, Corps Gras, Lipides*, 1998, **5**, 391–395.

View Article Online

Published on 11 November 2011. Downloaded by Michigan State University on 19/01/2016 06:25:56.

138 E. Deffense, *Eur. J. Lipid Sci. Technol.*, 2000, **102**, 234–236.
139 E. Deffense, *Agro Food Ind. Hi-Tech*, 2008, **19**, 67–68.
140 R. G. Larson, *The Structure and Rheology of Complex Fluids*, Oxford University Press, Oxford, 1999.
141 R. O. Feuge, W. Landmann, D. Mitcham and N. V. Lovergren, *J. Am. Oil Chem. Soc.*, 1962, **39**, 310–313.
142 S. V. Vaeck, *Fette, Seifen, Anstrichm.*, 1960, **62**, 709–722.
143 E. Windhab, E. A. Niediek and L. Rolfes, *Süsswaren Technik und Wirtschaft*, 1993, **3**, 32–37.
144 G. Ziegleder, *ZFL, Intern. Z. Lebensm.-Technol. Verfahrenstech.*, 1985, **36**, 412–416.
145 S. Bolliger, B. Breitschuh, M. Stranzinger, T. Wagner and E. J. Windhab, *J. Food Eng.*, 1998, **35**, 281–297.
146 S. Bolliger, Y. T. Zeng and E. J. Windhab, *J. Am. Oil Chem. Soc.*, 1999, **76**, 659–667.
147 J. Briggs and T. Wang, *J. Am. Oil Chem. Soc.*, 2004, **81**, 117–121.
148 S. D. MacMillan, K. J. Roberts, A. Rossi, M. A. Wells, M. C. Polgreen and I. H. Smith, *Cryst. Growth Des.*, 2002, **2**, 221–226.
149 B. D. Cullity and S. R. Stock, *Elements of X-Ray Diffraction*, Prentice Hall, New Jersey, 2001.
150 G. Mazzanti, S. E. Guthrie, A. Marangoni and S. H. J. Idziak, *Cryst. Growth Des.*, 2007, **7**, 1230–1241.
151 G. Mazzanti, S. E. Guthrie, E. B. Sirota, A. G. Marangoni and S. H. J. Idziak, *Cryst. Growth Des.*, 2004, **4**, 409–411.
152 G. Mazzanti, A. G. Marangoni and S. H. J. Idziak, *Phys. Rev. E: Stat., Nonlinear, Soft Matter Phys.*, 2005, **71**, 135–144.
153 G. Mazzanti, A. G. Marangoni and S. H. J. Idziak, *Eur. Phys. J. E*, 2008, **27**, 135–144.
154 G. Mazzanti, A. G. Marangoni and S. H. J. Idziak, *Food Res. Int.*, 2009, **42**, 682–694.
155 G. Mazzanti, S. E. Guthrie, A. G. Marangoni and S. H. J. Idziak, *Phys. Can.*, 2006, **62**, 313–320.
156 J. F. Toro-Vazquez, D. B. Perez-Martinez, E. A. Dibildox-Alvarado, M. A. Charo-Alonso and J. B. Reyes-Hernandez, *J. Am. Oil Chem. Soc.*, 2004, **81**, 195–202.
157 E. O. Afoakwa, A. Paterson and M. Fowler, *Trends Food Sci. Technol.*, 2007, **18**, 290–298.
158 E. O. Afoakwa, A. Paterson and M. Fowler, *Eur. Food Res. Technol.*, 2008, **226**, 1259–1268.
159 E. O. Afoakwa, A. Paterson, M. Fowler and J. Vieira, *Eur. Food Res. Technol.*, 2008, **227**, 1215–1223.
160 D. Dhonsi and A. G. F. Stapley, *J. Food Eng.*, 2006, **77**, 936–942.
161 S. Sonwai and M. R. Mackley, *J. Am. Oil Chem. Soc.*, 2006, **83**, 583–596.
162 E. M. Mudge and G. Mazzanti, *Cryst. Growth Des.*, 2009, **9**, 3111–3118.
163 S. E. Guthrie and S. H. J. Idziak, *Rev. Sci. Instrum.*, 2005, **76**, 026110.
164 S. E. Guthrie, PhD Thesis, University of Waterloo, 2008.
165 G. Mazzanti, S. E. Guthrie, E. B. Sirota, A. G. Marangoni and S. H. J. Idziak, in *Soft Materials—Structure and Dynamics*, ed. J. R. Dutcher and A. G. Marangoni, Marcel Dekker, New York, 1st edn, 2004, ch. 11, pp. 279–298.
166 B. Breitschuh and E. J. Windhab, *J. Am. Oil Chem. Soc.*, 1998, **75**, 897–904.
167 V. De Graef, K. Dewettinck, D. Verbeken and I. Foubert, *Eur. J. Lipid Sci. Technol.*, 2006, **108**, 864–870.
168 V. De Graef, B. Goderis, P. Van Puyvelde, I. Foubert and K. Dewettinck, *Eur. J. Lipid Sci. Technol.*, 2008, **110**, 521–529.
169 M. L. Herrera and R. W. Hartel, *J. Am. Oil Chem. Soc.*, 2000, **77**, 1189–1195.
170 M. L. Herrera and R. W. Hartel, *J. Am. Oil Chem. Soc.*, 2000, **77**, 1197–1204.
171 S. Martini, M. L. Herrera and R. W. Hartel, *J. Am. Oil Chem. Soc.*, 2002, **79**, 1063–1068.
172 G. Mazzanti, E. M. Mudge and E. Y. Anom, *J. Am. Oil Chem. Soc.*, 2008, **85**, 405–412.
173 G. Mazzanti and E. M. Mudge, in *Magnetic Resonance in Food Science: Challenges in a Changing World*, ed. M. Guðjónsdóttir, P. Belton and G. Webb, RSC Publishing, Cambridge, UK, 1st edn, 2009, ch. 11, pp. 89–96.
174 *US Pat.*, PCT/CA2008/000594, 2008.
175 F. Maleky and A. G. Marangoni, *J. Food Eng.*, 2008, **89**, 399–407.
176 A. G. Marangoni, D. M. Tang and A. P. Singh, *Chem. Phys. Lett.*, 2006, **419**, 259–264.
177 F. Maleky and A. G. Marangoni, *Soft Matter*, 2011, **7**, 6012–6024.
178 G. Ziegleder and I. Schwingshandl, *Fett/Lipid*, 1998, **100**, 411–415.
179 R. Campos, PhD Thesis, University of Guelph, 2005.
180 D. S. Grall and R. W. Hartel, *J. Am. Oil Chem. Soc.*, 1992, **69**, 741–747.
181 M. E. Miquel, S. Carli, P. J. Couzens, H. J. Wille and L. D. Hall, *Food Res. Int.*, 2001, **34**, 773–781.
182 S. Marty, K. Baker, E. Dibildox-Alvarado, J. N. Rodrigues and A. G. Marangoni, *Food Res. Int.*, 2005, **38**, 1189–1197.
183 R. S. Khan and D. Rousseau, *Eur. J. Lipid Sci. Technol.*, 2006, **108**, 434–443.
184 G. Ziegleder, C. Moser and J. Geier-Greguska, *Fett/Lipid*, 1996, **98**, 253–256.
185 G. Ziegleder, C. Moser and J. Geier-Greguska, *Lipid-Weinheim*, 1996, pp. 196–198.
186 V. Gekas, *Transport Phenomena of Foods and Biological Materials*, CRC Press, Boca Raton, 1992.
187 D. C. Scott, *Pharm. Res.*, 2001, **18**, 1797–1800.
188 C. Yang, W. Smyrl and E. I. Cussler, *J. Membr. Sci.*, 2004, **230**, 183–188.
189 N. Epstein, *Chem. Eng. Sci.*, 1989, **3**, 777–779.
190 R. M. Barrer, in *Diffusion in Polymers*, ed. J. Crank and G. S. Park, Academic Press, New York, 1st edn, 1968, ch. 6, pp. 165–217.
191 E. I. Cussler, *J. Membr. Sci.*, 1990, **52**, 275–288.
192 J. Crossley and J. Aguilera, *J. Food Process Eng.*, 2001, **24**, 161–177.
193 R. J. Love, PhD Thesis, Massey University, New Zealand, 2003.

 This journal is © The Royal Society of Chemistry 2012